E.O. Paton Electric Welding Institute of the National Academy of Sciences of Ukraine

International Scientific-Technical and Production Journal

The Paton WELDING JOURNAL

Issue 04 2019

Published Monthly Since 2000

English translation of the monthly «Avtomaticheskaya Svarka» (Automatic Welding) journal published in Russian since 1948

Address
E.O. Paton Electric Welding Institute,
International Association «Welding»
11 Kazimir Malevich Str. (former Bozhenko Str.),
03150, Kyiv, Ukraine
Tel.: (38044) 200 60 16, 200 82 77
Fax: (38044) 200 82 77, 200 81 45
E-mail: journal@paton.kiev.ua
www.patonpublishinghouse.com

State Registration Certificate
KV 4790 of 09.01.2001
ISSN 0957-798X
DOI: http://dx.doi.org/10.15407/tpwj

Subscriptions
$384, 12 issues per year,
air postage and packaging included.
Back issues available.

CONTENTS

DOI: http://dx.doi.org/10.15407/tpwj2019.04.01

INFLUENCE OF PARAMETERS OF ELECTRODYNAMIC TREATMENT ON RESIDUAL STRESSES OF WELDED JOINTS OF ALLOY AMg6

L.M. LOBANOV, N.A. PASHCHIN, A.N. TIMOSHENKO, O.L. MIKHODUJ, P.V. GONCHAROV and **A.V. CHERKASHIN**
E.O. Paton Electric Welding Institute of the NAS of Ukraine
11 Kazimir Malevich Str., 03150, Kyiv, Ukraine. E-mail: office@paton.kiev.ua

The influence of parameters, determining the different duration of electrodynamic effect on reduction of level of residual stresses in welds of butt joints of aluminium alloy AMg6 as a result of electrodynamic treatment, was investigated. It is shown that the increase in electrodynamic effect duration, attained by the increase in inductance of a discharge circuit at constant amplitude values of a pulsed electric current, is characterized by a higher increase in time of current decay as compared with the period of its growing. At the same time, the increase in duration of electrodynamic effect leads to the increase in the method efficiency for reducing the level of residual stresses in welded joints of AMg6 alloy. It is noted that at the duration of $t \geq 0.7$ms the reduction in stresses is determined by the electromagnetic effect intensity and Joule heating of the plate surface. 5 Ref., 1 Table, 4 Figures.

Keywords: *electrodynamic treatment, aluminium alloys, electric current pulse, residual welding stresses, electrodynamic effect duration*

The methods of treatment of metallic materials and welded joints by the effect of pulsed electromagnetic fields have found spreading since the 2000s in regulation of a stressed state of the structure elements [1].

One of these methods is the electrodynamic treatment (EDT), based on the combined effect of a pulsed electric current and dynamic pressure on the welded joint. The electrodynamic effect on metal at EDT is realized by a contact of the working electrode to the metal surface at the moment of discharge of a capacitive energy storage. As a result of a combined effect of the dynamic load and pulsed electric current (PEC) the electric pulsed processes, connected with an electroplastic effect (EPE)[1], as well as dynamic processes, defined by the formation of elastic waves of deformations in the material, are initiated in the metal treated. The result of the combined proceeding of electroplastic and dynamic processes are the change in the stressed state of welded joints. The investigations were carried out on evaluation of effect on the efficiency of processing of such parameters of electrodynamic effect, as charging voltage and storage capacity, amplitude values of a pulsed current and dynamic pressure [2]. For all this, the system investigations of influence of duration of electrodynamic effects on EDT efficiency were not carried out until now. However, in accordance with data of works [3, 4], the duration of electric pulsed and dynamic effects, jointly defining the EDT controlling mechanism, has an influence on the stressed state level in structural materials. Coming from the above-mentioned, the study of influence of duration of electromagnetic effects on stressed state of welded joints seems to be rather urgent.

The aim of the present work was the investigation of influence of duration of electrodynamic effect at EDT, as well as the parameters, defining it, on stressed state of welded joints of aluminium alloy AMg6.

Procedure of carried out experiments. The influence of duration of electrodynamic effect at EDT on stressed state of 400×100×2 mm specimens of welded butt joints of alloy AMg6, made by automatic TIG (Ar) welding at the following values of arc voltage, welding current and process speed, respectively: U_w = 20 V, I_w = 170 A and v_w = 5.5 mm/s, was investigated.

To generate the electrodynamic effects, the source of a pulsed electric current (SPEC) with a variable inductance L was used, which was designed on the base of discharge-capacitor systems. The step adjustment of inductance allows changing the PEC duration t and, as a consequence, the intensity of electrodynamic effects [2].

To realize EDT, the electrode device (ED) was used, the appearance of which is shown in Figure 1. The working organ of ED is electrode *1*, the end of which during EDT contacts the welded joint surface. Electrode is fixed in a collet chuck *2*, mounted in a

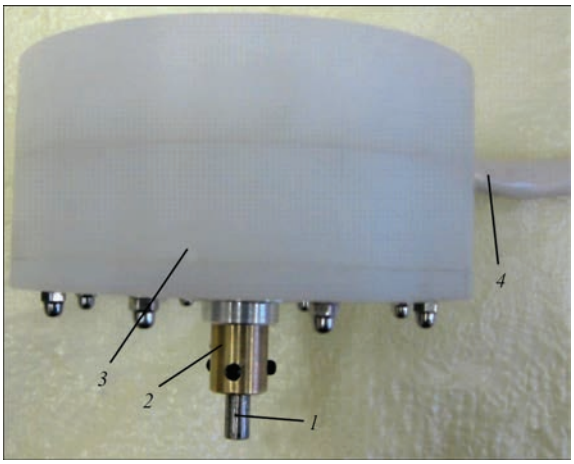

Figure 1. Electrode device for EDT (see designations in the text)

protective casing *3*, which contains the device, providing the effect of electric pulsed and dynamic components of EDT on the welded joint. Power cable *4* provided connection of ED to SPEC.

The EDT (Figure 2) of external surface and root of weld of test specimens was carried out. The treatment was made in the conditions of a «rigid fixation». To realize if the surface of plate *2* before EDT was fixed by a distributed load *q* on the assembly plate *3*, avoiding possible angular deformations of the specimen. This scheme of fixation, according to [5], provided the maximum efficiency of the electrodynamic effect at other equal parameters of the EDT mode. To realize EDT, ED *1* was mounted on the weld surface and provided its guaranteed electrical contact at closing the discharge circuit.

By switching-on of power switch K the discharge of capacitive energy storage C through ED into material treated was initiated. The time distributions of pulsed current *I* were recorded by using Hall sensor *4*, built-in into the discharge circuit, as shown in Figure 3. During EDT fulfillment the ED was moved over the weld surface at 3 mm step. The number of electrodynamic effects provided the electroplastic deforming of the region treated.

The effect of EDT parameters on change in longitudinal (along the weld line) component σ_x of residual stressed state of welded plates of alloy AMg6 at equal amplitude values of pulsed current *I* and variations of *t* was investigated**.** Equality of values *I* at different duration of effect *t*, preset by change in *L*, provided the growth in values of charge voltage U_{ch}. As a basic

Parameters of EDT of welded plates of alloy AMg6 of 400×100×2 mm sizes

No.	Inductance *L*, μH	Voltage of PEC U_{ch}, V	Amplitude of PEC *I*, kA	Duration of PEC *t*, ms	Energy of PEC E_s, J
1	5.3	185	1.0	0.7	94
2	20	388	1.0	1.75	413
3	71.5	726	1.0	4.5	1449

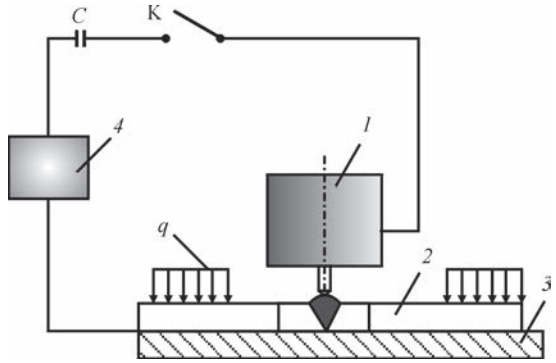

Figure 2. EDT of specimens of welded joints of alloy AMg6 at «rigid» fixation: *C* — capacitive energy storage; K — power switch; *q* — fixing load; *1* — ED; *2* — specimen; *3* — assembly plate; *4* — Hall sensor

amplitude value of the pulsed current *I*, *I* = 1.0 kA was selected. Growth in U_{ch} resulted in increase of stored energy of charge E_{ch}.

Using the method of electron speckle-interferometry the values σ_x in weld center of welded plates were determined in initial state and after EDT [2].

Results of experiments and their discussion. The modes of EDT of plates at growth in values *L* and U_{ch}, providing *I* = 1.0 kA at accompanying increase in effect duration *t* and stored energy E_{ch}, are given in Table.

The time distributions of a pulsed current *I* of equal amplitude, corresponding to different effect duration *t*, are given in Figure 3. By analyzing the data of Table and Figure 3, it can be seen that increase in *L* leads to the growth in *t*. Here, the growth of *L* has the greatest influence on time of decay and duration of *t* of PEC, than on time of its growth, that is especially noticeable in comparison of curves *2* and *3*. At the same time, according to [4], namely in the phase of growth the dynamic effect has the most noticeable influence on stress-strain state of metallic materials.

Value σ_x in the weld center in initial state (without EDT) is determined by column 4 in Figure 4, where it is seen that the initial level of residual welding stresses reached 100 MPa. A low level of σ_x before treatment is explained by a small width of used plates.

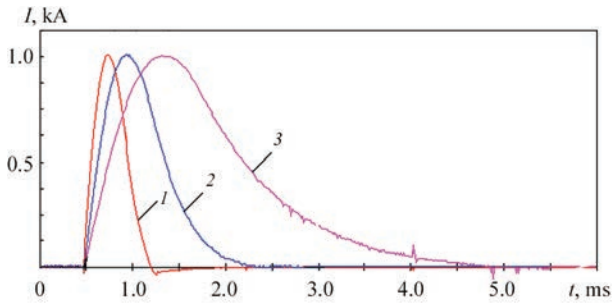

Figure 3. Time distribution of pulsed current *I* of equal amplitude at EDT of welded plates of alloy AMg6 of 400×100×2 mm sizes, where numbers of curves correspond to numbers of Table lines

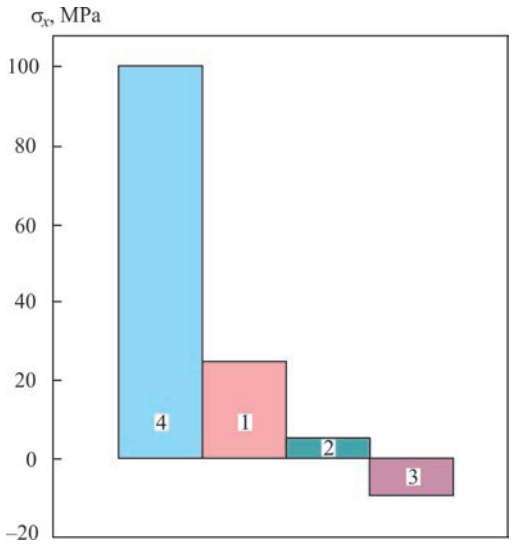

Figure 4. Peak values of stresses σ_x in weld center of welded plate of alloy AMg6 of 400×100×2 mm size, where numbers of columns *1–3* of values σ_x correspond to numbers of curves in Figure 3 (column 4 — σ_x without EDT)

During EDT at a mode, corresponding to minimum inductance (Figure 3, curve *1*), the decrease in stresses is observed in the treatment zone to 22 MPa (column 1). With increase in L (curve *2*) σ_x in the treatment zone is decreased almost to zero values (column *2*). At the further increase in L (column *3*) the stresses are transferred to the compression region, and values σ_x are close to k – 10 MPa (curve *3*). By analyzing the data of Table and Figures 3 and 4, it can be concluded that with the growth in L the effect is increased.

It should be noted, that the increase in EDT efficiency is determined by growth of values E_{ch}, required for keeping conditions I = 1 kA at large values L and, respectively, larger duration period t. In addition**,** during EDT at modes, corresponding to lines 2 and 3 of Table, there was a local fusion of metal in the zone of contact interaction of electrode with plate surface, being treated, due to the Joule heating [1]. Thus, the conclusion can be made, that at EDT of duration $t > 0.7$ ms, the decrease in level of residual stresses is determined by an electrodynamic effect under the conditions of a local Joule heating of the plate surface.

It should be noted that positive EDT effect on stressed state of welded plates under conditions of high levels of PEC energy is accompanied not only by heating, but also a local damage of the surface treated, which has a negative influence on the cyclic strength of alloy AMg6 [5]. Thus, it can be concluded that the increase in temperature in the zone of PEC effect it is possible to increase the EDT efficiency, avoiding its negative influence on the surface quality. Therefore, the application of EDT directly in the process of welding seems to be promising, that will be future direction of our further investigations.

Conclusions

1. On the basis of the developed procedure the influence of parameters of electrodynamic effect for reducing the level of residual stresses of welded joints of aluminium alloy AMg6, as a result of EDT, was investigated.

2. It was found, that increase in level of electrodynamic effect energy leads to increase in EDT efficiency for regulation of level of residual stresses in welds of butt joints of alloy AMg6. It is shown that at duration of current pulse for more than 0.7 ms the level of stresses is defined by the treatment intensity under conditions of the Joule heating.

3. It is rational, to carry out the further investigations for determination of efficiency of EDT application directly in the welding process.

1. Baranov, Yu.V., Troitsky, O.A., Avramov, Yu.S., Shlyapin, A.D. (2001) *Physical principles of electropulse and electroplastic treatments*. Moscow, MGIU [in Russian].
2. Lobanov, L.M., Pashchin, N.A., Cherkashin, A.V. et al. (2012) Efficiency of electrodynamic treatment of aluminium alloy AMg6 and its welded joints. *The Paton Welding J.*, **1**, 2–6.
3. Strizhalo, V.A., Novogrudsky, L.S., Vorobiov,E.V. (2008) *Strength of materials at cryogenic temperatures taking into account electromagnetic fields*. Kiev, IPS [in Russian].
4. Belova, M.M., Protsenko, S.S., Ivanov, A.V. (1987) Dynamics of deformation of elastic-plastic layer in impulse energy release. *Problemy Prochnosti*, **12**, 87–91 [in Russian].
5. Lobanov, L.M., Pashchin, N.A., Yashchuk, V.A., Mikhoduj, O.L. (2015) Effect of electrodynamic treatment on fracture resistance of aluminium alloy AMg6 under cyclic loading. *Ibid*., **3**, 91–98 [in Russian].

Received 24.01.2019

DOI: http://dx.doi.org/10.15407/tpwj2019.04.02

STRESS CONCENTRATION IN BUTT WELDED JOINTS WITH REINFORCEMENT FROM ONE SIDE (Review*)

A.V. MOLTASOV, P.M. TKACH, I.G. TKACH and **V.V. VERUSHKIN**
E.O. Paton Electric Welding Institute of the NAS of Ukraine
11 Kazimir Malevich Str., 03150, Kyiv, Ukraine. E-mail: office@paton.kiev.ua

The strength of parts and structural elements in the presence of welds largely depends on the design of their joints and assemblies. A sharp change of geometry in their vicinity causes the appearance of additional local stresses or their concentration. The value of these stresses depends on the structural shape of mating of separate elements. That is why they can affect the strength of welded structures in a different way. Stress concentration in the zone of transition from the weld to the base metal has a significant effect on joints fatigue resistance. At the elastic deformation, the theoretical stress concentration factor serves as a quantitative measure of stress concentration. It does not depend on properties of the material, and at a preset type of deformation its value is influenced only by geometry parameters of the stress concentrator, such as its shape and relative dimensions. In practice, the theoretical stress concentration factor is determined by approximate dependencies, as well as by analytical, experimental and numerical methods for investigation of stressed state. The description and analysis of these methods are the aim of the presented review. 37 Ref., 2 Figures.

Keywords: *butt welded joint, reinforcement from one side, axial load, stressed state, tension, bending, stress concentration*

At static loading effect of concentration is insignificant, since failure takes place under effect of stresses that exceed yield point of part material, and it is preceded by considerable plastic deformations, due to which inhomogeneity of stress distribution is reduced on contour as well as part section. However, great number of machine parts and elements of structures of general and special designation take up during operation a lot of changes of temporary loads, for example, moving cargos, transport, waves, wind etc. Changing loads that appear at that can provoke fatigue fracture of these structural elements.

Fatigue fracture differs from static one by the fact that it can be a consequence of application of not high stresses, sometimes significantly smaller than the yield point (multicycle fatigue), therefore, usually it takes place without noticeable preliminary macroplastic deformation. Therefore, effect of stress alignment, after reaching the yield point, is absent, so cyclic loads are sensitive to stress concentration, and various types of grooves, fillets, holes, undercuts, transitions of welds to base metal etc. are the potential places of preliminary nucleation of fatigue cracks.

In butt welded joints formation of a zone of higher loads is caused by weld reinforcement, and technology and mode of welding determine its main parameters. Thus, appearance and size of weld in arc welding depend on a method of welding, welding consumables, type of groove preparation, etc. For example, according to GOST 14771-76 C7, C25, C26 and C27 joints have similar reinforcement size on face and root sides and C2, C4, C9, C17, C18 and C22 joints can be made without reinforcement on the root side, i.e. they can be reinforced from one side.

The main geometry parameters of butt welds are width g and height h of weld reinforcement, fillet angle θ and radius of transition from weld to base metal r (Figure 1). Width and height of the reinforcement determine a general profile of butt weld, whereas fillet angle and radius of transition from weld to base metal characterize sharpness of concentrator in the local zones [1]. Therefore, in the case of ideal butt welded joint without such defects as linear and angular deformations in process of welding, a theoretical stress concentration factor (SCF) is determined by two independent constituents, first of which (structural SCF) $\alpha_{\sigma g}$ is provoked by general geometry of weld-

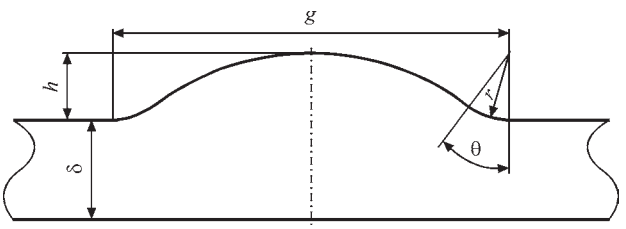

Figure 1. Main geometry parameters of butt welded joint with reinforcement from one side

*The publication contains the results of investigations carried by grant of the President of Ukraine and completive project F75 of the State Fund of Fundamental Investigations.

ed assembly and thickness of joining elements, and second (local SCF) $\alpha_{\sigma w}$ is the geometry of transition zone from weld to base metal [2]. Then, the maximum stresses σ_{max} will be determined by formula

$$\sigma_{max} = \alpha_{\sigma g}\alpha_{\sigma w}\alpha_{nom}, \quad (1)$$

where σ_{nom} is the nominal stresses that act at a distance from concentrator.

In practice such an approach is realized in a hot point stress method, which was developed by the researchers of The Welding Institute, in particular, Maddox S. J and Niemi E. [3, 4], and German researcher A. Hobbacher to solve the problems of fatigue strength of welded assemblies. Effect of general joint geometry and geometry of mating zone of weld to plates being welded on life of structural element for given variable loading in the indicated method are considered separately in calculations.

Since a stress gradient in zone of transition of weld to base metal is very high, the stresses calculated using a finite element method (FEM) in this zone are very sensitive to size of finite element grid [6]. Therefore, the structural constituent of stresses caused by general geometry of the joint is determined applying a computer model of investigated welded assembly, which does not include weld, by means of extrapolation of stresses calculated in the reference points at some distance form the weld. In particular, at linear extrapolation the reference points are located at 0.5δ and 1.5δ distance from the fusion line of weld to base metal on joint surface.

Number of cycles before failure of assembly at preset value of variable load can be obtained by marking a found value of a range of structural stresses, i.e. which were determined by structural SCF $\sigma_{\alpha g}$, on a fatigue curve for butt welded joint in FAT (File Allocation Table) catalogue. Application of these catalogues in calculations allows taking into account effect of weld, since these catalogues contain series of fatigue curves obtained by the results of fatigue tests of real welded elements and expressed in values of the range of nominal stresses independent on a factor of cycle asymmetry at load application [7].

Obviously, that the fatigue curves of the real welded joints take into account effect on fatigue resistance of residual welding stresses and mechanical inhomogeneity of regions on heat-affected zone, but this approach does not provide the possibility to determine local stressed state in some vicinity of the stress concentrator. Therefore, the methods based on determination of effective local SCF $K_{\sigma w}$ are used in the fatigue calculations. It depends not only on geometry shape of transition zone from weld to base metal, but also from some constants of the material, such as factor of sensitivity to stress concentration [1], critical distance [8] or size of structural element [9].

The most widespread is application of a practice for determination of effective local SCF in form of a method of factious rounding of stress concentrator proposed by German researcher D. Radaj [10]. This method is based on the assumption that in calculation of theoretical local SCF $\sigma_{\alpha w}$ the value of actual radius of concentrator curvature is taken, and the value of factious radius, which is determined by minimum dimensions of structural element and rigidity of stressed state [11], are taken for calculation of effective local SCF $K_{\alpha w}$.

Based on the results of fatigue testing of over 1000 samples of welded joints of different shape and size it is determined that a joint radius of the effective concentrator for steel makes 1 mm [12]. Evaluations of effective local SCF, as a rule, are made based on known theoretical local SCF, and its real value is determined experimentally as a relationship of endurance limit of smooth sample to endurance limit of sample with stress concentrator [1]. So, application of a universal factious radius for whole class of materials can provide the results different from the experiment.

It is necessary to remember that the considered method can be used only for determination of fatigue resistance characteristics, however, the experience shows that stress concentration shall be taken into account not only at effect of vibration loading, but at static loading and impact, if brittle fracture of the structure is possible. Thus, at operation of welded joints under low temperature conditions the transition of metal into a brittle state depends on the operating temperature as well as other factors, in particular, on stress concentration. The latter for structures of cryogenic engineering is one of the most important factors that determine their strength and life [13]. Therefore, evaluation of the theoretical local SCF is one of the main measures for preliminary fracture of welded assemblies and structure elements.

Analytical strength calculations of welded joints based on the methods of material resistance do not consider the peculiarities of conditions of stress distribution in the places of change of structure element shape, therefore they can not be used for solution of the problems of stress concentration determination.

The elasticity theory, which is free of many assumptions accepted for simplification in material resistance, allows solving the problems, which are out of limit range applied by these assumptions, and is more general theory, but at the same time is more compound, and its application in many cases is accompanied by complex calculations.

The problem can be significantly simplified in a series of cases using a method of sections. It lies in a division of complex welded joint on a series of simple elements with replacement of weld reinforcement by equivalent work of corresponding forces that allows using known in advance solutions of elasticity theory.

Due to weld reinforcement in the area of increase of transverse sections the projecting parts limit the deformations of main elements of joint. This provokes local distortion of sections and change of the conditions of distribution of power flow. Limiting effect of the projections can be considered equivalent to the effect of some surface horizontal forces, which are tangential stresses applied in the reinforcement place [14].

Using a method of sections it is possible to eliminate the local reinforcement and replace their effect by work of equivalent forces, and then the calculation scheme of welded joint can be presented in form of a main element of constant transverse section without shape change. It in addition to external load is also effected by some more forces applied in the points of imaginary detachment of the projecting parts (Figure 2).

Knowing the law of distribution of equivalent forces it is possible to use already known solutions in the elasticity theory as for band loaded at the edges or ends with distributed normal or tangential forces [15] and determine normal stresses in the places of geometry inhomogeneity of butt welded joint.

Closed-form solution of the problem was obtained in work [14] using the method of sections for simplified model of butt joint with rectangular reinforcement.

Consideration of curvilinear shape of the projections of real butt welds significantly complicates differential equation for determination of equivalent tangential stresses, applied in the place of conventional detachment of projection. Even using simplified model of projection in form of symmetric relatively to weld axis inclined straight lines [14] this equation appears to be a linear inhomogeneous differential equation of second order with variable factors.

Fulfillment of the requirements at the boundary with the projection similar by shape to butt weld reinforcement is possible in curvilinear coordinates, but then the problem appears with meeting the conditions at straight line boundary. Therefore, for the first time German researcher H. Neuber has found an analytical solution of the plane problem of elasticity theory as for tension of semi-infinite plate with the projection [9]. He selected such a system of orthogonal curvilinear coordinates that one of the coordinate lines develops a projection, and stress function, which satisfies problem boundary conditions, was determined. The maximum stresses on the joint contour and geometry of the projection were determined through the contour line parameter, however, it is impossible to set a feedback between this parameter and sizes of the projection. Therefore, dependence of the maximum stress on g/r relationship is presented in form of diagram. It is necessary to take into account that this diagram can only be used for projections with $g/2r \geq 4\sqrt{3}$ relationship. It is related with the fact that a half-width of the projection is a distance from its symmetry axis

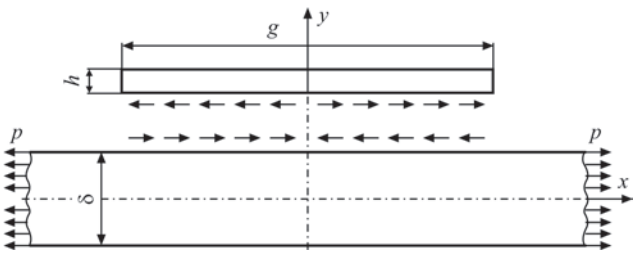

Figure 2. Scheme of loading of separate parts of model of butt welded joint with rectangular projection

to point, in which the contour is parallel to this axis. In the projections, size of which does not meet this requirement, such a point is absent in general, and the contour parameter is a complex number. Thus, it is impossible to determine the maximum stresses in this range [16].

Besides, the dependence of the maximum stress on g/r relationship stipulates increase of the maximum stress not only with decrease of radius of weld to base metal transition, but with increase of width of projection that is not provided by experimental data. In particular, in work [17] for the simplified models of welded joint with $r = 0.5$ and $h = 5$ mm it was determined using a polarization-optical method that a value of local SCF at axial tension with increase of weld width from 5 to 25 mm reduces from 1.60 to 1.59, and its maximum value 1.61 was registered at $g = 8$ mm. Such insignificant deviations of local SCF values to increase as well as decrease side, are more likely related with the measurement error or deviation of other geometry sizes of the models that can make a basis for conclusion that it does not depend on projection width.

A single parameter of the contour line, which in work [9] set the sizes and shape of the projection, does not allow setting main geometry characteristics of weld reinforcement independent one from another. Therefore, in work [18] more general problem of elasticity theory was solved using conformal mapping method. A mapping function was set in form of series, keeping the larger number of terms of which it is possible to reduce the radius of projection mating with the plate, and varying the factors at its terms change the h/g relationship.

The disadvantage of such approach is the fact that size and shape of the projection, as in [9], are determined by the parameters of contour line that are set by mapping function. Therefore, an approximation formula for determination of local SCF in the butt welded joint of sufficiently large thickness can be determined only by means of statistical processing.

Since in conformal mapping of a region defined by unit circle or region that lies out of this circle on closed polygonal obtaining the region with set relative size is sufficiently difficult problem, therefore, in order to take into account effect of all parameters that determine shape of real welded joints, on stressed

state, it is necessary to analyze the functions with considerably large number of series terms.

A formula for determination of theoretical local SCF was obtained thanks to application of a numerical algorithm of conformal mapping of set singly-connected regions by a method of joint interpolation of coordinates of node points and plotting the mapping functions on large number of these points in work [19] by means of approximation of analytical solutions. However, according to this formula given SCF reduces with rise of thickness of plates being joined, that is not proved by the results of calculations using FEM [20], which showed that the local stresses rise with increase of thickness.

Uncertainty of the results obtained using such an approach as for final regions of types of plates of variable thickness is explained by the fact that presenting the mapping functions in form of a series can provoke appearance of variations of contour stresses due to insufficient smoothness of the obtained contour. Therefore, consideration of effect of the plate thickness was achieved by means of processing of additional experimental data that allowed obtaining the formula [21]

$$\alpha_{\sigma w} = 1 + \frac{1}{\sqrt{r\left(\frac{14}{g} + \frac{1.7}{h} + \frac{5}{\delta}\right)}}. \qquad (2)$$

Development of computer engineering and numerical methods for solution of elasticity theory problems, in particular, FEM resulted in the fact that traditional experiments on determination of stressed state in the zones of concentration on full-scale samples were replaced by numerical experiments based on finite element models. Statistical processing of the results of analytical or numerical solutions of elasticity theory problems or experimental data provides the possibility to get empirical dependencies for determination of local SCF, which have general view

$$\alpha_{\sigma w} = 1 + Ar^{-n}, \qquad (3)$$

where A is the parameter that takes into account macrogeometry of the joint and conditions of its loading.

Large amount of proposed dependencies of type (3) provokes some difficulties in solution of the issue, which of them should be used in each specific case. Thus, following data of review [22] the index of level n in these dependencies is changed in 0.3–0.67 range.

Authors of work [23] by means of corresponding statistical processing of the calculation results using the most widely used formulas of theoretical local SCF at set values of numerical parameters, which characterize shape of weld, determined that Berezovskii–Bakshi formula is the most versatile at variation in wide range of geometry parameters and recommended for practical application

$$\alpha_{\sigma w} = 1 + \left(\frac{r}{h\tan(\theta/2)} + 4\frac{r}{\delta} + 5\frac{r}{r+g}\right)^{-\frac{2}{3}}, \qquad (4)$$

which for butt welded joints with reinforcement from one side provides the reliable result at relationships $r/\delta = 0.01–0.1$ and $h/\delta = 0.1–0.2$.

The problem is in the fact that thin-sheet joints do not correspond to reliability fields for this and other formulas analyzed in work [23]. Thus, for butt welded joints of type C7 according to GOST 8713–79 at thickness of welded plates $\delta = 2–3$ mm the reinforcement height h can vary in 0.5–2.5 mm range, respectively h/δ relationship lies in 0.17–1.25 range.

Irrelevance of calculation data, obtained at empirical formulas from work [23], to a zone of «reliable recommendations» at tension of small thickness welded joints, asymmetric relatively to axis of application of external loading, can be explained by additional bending, promoted by this asymmetry.

These circumstances were outlined by Belarusian researcher Yu.O. Tsumarev in work [24], where he indicated that presence of bending stresses in thin-sheet welded joints with reinforcement from one side results in significant rise of sum stresses in the root part and its decrease in the face part of weld. Based on data of this work axial tension of 200 MPa loading of butt welded joint with h/δ – 0.5 relationship provokes the maximum stresses of 240 MPa in a zone of weld to base metal transition and in the root part in a region with reinforcement it is 260 MPa. Obviously, that the maximum stresses in a weld to base metal transition zone can be determined using local SCF $\alpha_{\sigma w}$, calculated by any of the formulas given in [23]. However, the maximum stresses act on the root side, where local stress concentrator is absent ($\alpha_{\sigma w} = 1$), and additional bending stresses are taken into account with the help of structural SCF $\alpha_{\sigma g}$, which according to [25] is determined by formula

$$\alpha_{\sigma g} = \frac{\delta(\delta + 4h)}{(\delta + h)^2}. \qquad (5)$$

The results of calculation of Yu.O. Tsumarev are proved by the experimental data accumulated during many years in a department of strength of welded joints at the E.O. Paton Electric Welding Institute of the NAS of Ukraine as a result of multicycle fatigue testing of butt welded joints of aluminum alloys. They showed that initiation of fatigue fracture is sometimes started from the root side of weld in thin-sheet butt joints with reinforcement from one side.

Work [25] for determination of stresses on the root side of the weld σ_r proposed a formula

$$\sigma_r = P\frac{\delta + 8e}{(\delta + 2e)^2}, \qquad (6)$$

where P is the axial load that acts on unit of width of welded joint; e is the eccentricity of applied axial loading.

Following the manipulations of work [25] the stresses on the face side of weld (α_f) can be determined by formula

$$\sigma_f = P\frac{\delta - 4e}{(\delta + 2e)^2}. \quad (7)$$

Analysis of this formula shows that it really does not take into account geometry parameters of the zone of weld to base metal transition and increase of stresses on face side of the joint, which, as it is known, for fulfillment of equilibrium conditions in the corresponding sections have to be compensated by some decrease of stresses on the root side. Therefore, the real pattern of stress fields is often determined using FEM computer modelling. However, the significant disadvantage of such approach is the fact that modelling varies height and width of reinforcement [26] and smooth transition on radius from weld metal to base metal is not modeled, regardless the known fact that this radius has a dominant effect on value of the maximum stress [27, 28].

If local SCF is calculated without consideration of fillet radius then it most likely will characterize not a stressed state of welded joint, but finite element grid [29]. Besides, at presence of sharp concentrators, application of local SCF does not seem to be perspective due to singularity of stresses in their vicinity [30]. In such a case, weld to base metal transition zone can be presented from point of view of fracture mechanics as angular cutoff with known distribution of stresses close to its tip [31].

Amount of finite elements necessary to get reliable results is very large at small relative radiuses of transition from weld to base metal (side of element not more than 10 % of radius). Performing the calculations with such detailed approximation of elements is sufficiently difficult. Such calculations require application of high efficiency computation equipment and are carried out only in the exceptional cases [33]. Therefore, to reduce the calculation volume for welded joint it is reasonable to use mathematical formulas for determination of $\alpha_{\sigma w}$ factor, and $\alpha_{\sigma g}$ factor was calculated using FEM and available system of engineering analysis [34].

In the case of action of tensile stresses as well as bending stresses it is impossible to use formula (1), since current procedures [35, 36] lie in determination of structural tensile and bending stresses with further multiplication of each of them on corresponding SCF. Thus, in work [36] it was proposed to decompose the stresses, distributed on the thickness, on tensile-compression stresses (membrane stress) α_m and bending stresses α_b and determine the maximum stresses on formula

$$\sigma_{\max} = \alpha^m_{\sigma w}\sigma_m + \alpha^b_{\sigma w}\sigma_b, \quad (8)$$

where $\alpha^m_{\sigma w}$, $\alpha^b_{\sigma w}$ are the SCF at tension and bending, respectively.

Obviously that in this case it is no need to use structural SCF $\alpha_{\sigma g,}$ since bending stresses are taken into account separately.

Based on hypothesis of broken sections in work [37] there were developed an analytical method for investigation of local stressed state in the zones of stress concentration of butt welded joints with reinforcement from one side. It takes into account eccentricity of application of axial load and local geometry of weld to base metal transition zone. Applying this method the mathematical expressions for determination of stresses on a surface of transition zone of weld to base metal and on weld root side were obtained.

Conclusions

1. Theoretical SCF in butt welded joints is determined by two independent constituents, first of which (structural SCF) caused by general contours of welded assembly and thickness of elements being joined, and second (local SCF) is the geometry of weld to base metal transition zone.

2. Bending stresses, which are taken into account by structural SCF, act as structural constituent of stresses at tension of butt welded joints with reinforcement from one side. If height of reinforcement is comparable with thickness the plates being joined, that is typical for thin-sheet joints, the sum stresses due to tension and bending at weld root side, regardless the absence of local concentrator, can be higher than in the weld to base metal transition zone.

3. Structural SCF for conventional shape of reinforcement can be determined analytically using the materials resistance method or FEM. Limitation of field of application of FEM is related with high labor intensity in designing the accurate, even 2D model with dense local grid. Therefore, for calculation of local SCF the empirical dependencies are used. They were obtained by means of statistical processing of the results of analytical and numerical solutions of problems of elasticity theory or experimental data.

4. Area of reliable and available for today calculation dependencies for determination of local SCF includes the possibility of their application for thin-sheet butt welded joints. Besides, numerical value of local SCF does not provide the information on redistribution of stresses on thickness of joint, in particular, on the weld root side due to their concentration in the weld to base metal transition zone. Therefore, the calculations of joints with reinforcement from one

side can not be limited only by SCF evaluation, and it is necessary to determine the stresses on the face and root sides of weld.

5. The combination procedures are the most effective for determination of stressed state in the vicinity of weld reinforcement. Following to them the stresses in the local zones of weld to base metal transition are determined by mathematical formulas obtained in analytical way and stresses at sufficient distance from the sharp concentrators applying FEM computer modelling.

1. Trufyakov, V.I., Dvoretsky, V.I., Mikheev, P.P. et al. (1990) *Strength of welded joints under alternating loads*. Ed. by V.I. Trufyakov. Kiev, Naukova Dumka [in Russian].
2. Gassner, E., Haibach, E. (1968) Die Schwingfestigkeit von Schweissverbindungen aus der Sicht einer oerlichen Beanspruchungsmessung. *Fachbuchreihe Schweisstechnik*, Bd 53. Tragfaehigkeitsermittlung bei Schweissverbindungen, Dusseldorf, Verlag Schweisstechnik, 47–73 [in German].
3. Maddox, S.J. (2003) Review of fatigue design rules for welded structures. *The Paton Welding J*., **10–11**, 94–99.
4. Niemi, E., Fricke, W., Maddox, S.J. (2006) *Fatigue analysis of welded components: Designer's guide to the structural hotspot stress approach*. Cambridge, Woodhead Publishing Ltd.
5. Hobbacher, A. (2008) *Recommendations for fatigue design of welded joints and components*. Paris, IIW.
6. *Yong* Bai, Wei-Liang Jin (2015) *Marine structural design.* Oxford, Elsevier Publishing.
7. Maddox, S.J. (1991) *Fatigue strength of welded structures*. Cambridge, Abington Publishing.
8. Herasymchuk, Oleg, Herasymchuk, Olena (2017) Theoretical estimation of fatigue life under regular cyclic loading. *Mechanics and Advanced Technologies*, 79(**1**), 49–56.
9. Neuber, H. (2001) *Kerbspannugslehre: Theorie der Spannungskonzentration Genaue Berechnung der Festigkeit*. Berlin, Springer-Verlag Berlin Heidelberg [in German].
10. Radaj, D., Sonsino, S.M., Fricke, W. (2006) *Fatigue assessment of welded joints by local approaches*. Cambridge, Woodhead Publishing Ltd.
11. Korostylyov, L.I., Litvinenko, D.Yu. (2016) Analysis and classification of methods for estimation of strength of welded thin-walled structures of hull. *Vestnik GUMRF Adm. S.O. Makarov*, **3**, 104–118 [in Russian].
12. Hobbacher, A.F. (2003) Effective notch stress method in comparison with other methods in fatigue design of welded structures. *The Paton Welding J*., **10–11**, 117–121.
13. Vorobiov, E.V., Strizhalo, V.A., Anpilogova, T.V. (2017) Strength of steels at cooling up to 4.2 K under conditions of stress concentration. *Problemy Prochnosti*, **5**, 5–10 [in Russian].
14. Navrotsky, D.I. (1968) *Design of welded structures taking into account stress concentration*. Leningrad, Mashinostroenie [in Russian].
15. Timoshenko, S.P., Goudier, J. (1975) *Theory of elasticity*. Ed. by G.S. Shapiro. Moscow, Nauka [in Russian].
16. Kopelman, L.A. (1978) *Resistivity of welded assemblies to brittle fracture*. Leningrad, Mashinostroenie [in Russian].
17. Trufyakov, V.I. (1973) *Fatigue of welded joints*. Kiev, Naukova Dumka [in Russian].
18. Karkhin, V.A. (1985) Influence of weld shape on stress distribution at tension of large-thickness butt joints. *Avtomatich. Svarka*, **9**, 25–28 [in Russian].
19. Turmov, G.P. (1976) Determination of stress concentration factor in welded joints. *Ibid*., **10**, 14–16 [in Russian].
20. Stakanov, V.I., Kostylyov, V.I., Rybin, Yu.I. (1987) On calculation of stress concentration factor in welded joints with butt and fillet welds. *Ibid*., **8**, 7–18 [in Russian].
21. Karkhin, V.A., Kopelman, L.A. (1976) Stress concentration in butt joints. *Svarochn. Proizvodstvo*, **2**, 6–7 [in Russian].
22. Tkacz, P., Moltasov, A. (2017) Rozwoj metod oceny stanu naprezenia w elementach konstrukcji spawanych. Czesc 1: Metody tradycyjne. *Biuletin Instytutu Spawalnictwa*, **4**, 52–56 [in Polish].
23. Makhnenko, V.I., Mosenkis, R.Yu. (1985) Calculation of stress concentration factors in welded joints with butt and fillet welds. *Avtomatich. Svarka*, **8**, 7–18 [in Russian].
24. Tsumarev, Yu.A. (2010) Influence of asymmetry of one-side butt welds on distribution of stresses in welded joint. *Svarka i Diagnostika*, **5**, 24–27 [in Russian].
25. Tsumarev, Yu.A. (2010) Influence of eccentric tension on stressed state of butt welded joint. *Svarochn. Proizvodstvo*, **6**, 6–10 [in Russian].
26. Ermolaev, G.V., Martynenko, V.A., Marunich, I.V. (2014) Effect of weld convexity sizes on stress state of butt joint during tension. *The Paton Welding J*., **8**, 26–32.
27. Gurney, T.R. (1979) *Fatigue of welded structures*. 2nd Ed. London, New York, Melbourne, Cambridge University Press.
28. Asnis, A.E., Ivashchenko, G.A., Anderson, Ya.E. (1982) Effect of weld to base metal transition radius on fatigue resistance of welded joints. *Avtomatich. Svarka*, **4**, 48–51 [in Russian].
29. Karkhin, V.A., Kostylyov, V.I., Stakanov, V.I. (1988) Effect of geometric parameters of butt, tee and cruciform joints on stress concentration factor. *Ibid*., **3**, 6–11 [in Russian].
30. Lukianov, V.F., Parkhomenko, A.A., Rogozin, D.V. (2010) Evaluation of fatigue strength of welded joints with fillet welds based on analysis of local stress state. *Svarka i Diagnostika*, **6**, 17–20 [in Russian].
31. Parton, V.Z., Perlin, P.I. (1981) *Methods of mathematical theory of elasticity.* Moscow, Nauka [in Russian].
32. Rybin, Yu.I., Stakanov, V.I., Kostylyov, V.I. et al. (1982) Study by finite element method of effect of geometric parameters of tee and cruciform welded joints on stress concentration. *Avtomatich. Svarka*, **5**, 16–20 [in Russian].
33. Kirian, V.I., Dvoretsky, V.I., Malgin, M.G. (2012) Calculation of local stresses in zones of welded joints of large-sized space structures. *The Paton Welding J*., **4**, 2–5.
34. Korostylyov, L.I., Litvinenko, D.Yu. (2015) Evaluation of stress concentration factor in welded assemblies of thin-walled structures by calculation of macro- and microconcentration. *Naukovyj Visnyk KhDMA*, 13(**2**), 184–194 [in Russian].
35. Moltasov, A.V., Klochkov, I.N., Knysh, V.V. (2013) Engineering approach of calculation of stress concentration factor in overlap welded joint at tension and bending. *Visnyk NTUU KPI. Seriya Mashynobuduvannya*, 69(**3**), 150–157 [in Russian].
36. Goyal, R., El-Zein, M., Glinka, G. (2016) A robust stress analysis method for fatigue life prediction of welded structures. *Welding in the World*, 60(**2**), 299–314.
37. Moltasov, A., Motrunich, S. (2017) Badania lokalnego stanu w obszarze niejednorodnosci geometrycznej doczolowych zlaczy spawanych z jednostronnym nadlewem. *Biuletin Instytutu Spawalnictwa*, **4**, 64–71 [in Polish].

Received 22. 01.2019

DOI: http://dx.doi.org/10.15407/tpwj2019.04.03

CALCULATION OF THERMAL FIELDS DURING JOINING ALUMINIUM PLATES THROUGH INTERLAYERS AT LOCAL HEATING OF THE JOINT ZONE

M.V. KULINICH[1], **T.V. ZAPOROZHETS**[2], **A.M. GUSAK**[2] and **A.I. USTINOV**[1]
[1]E.O. Paton Electric Welding Institute of the NAS of Ukraine
11 Kazimir Malevich Str., 03150, Kyiv, Ukraine. E-mail: office@paton.kiev.ua
[2]Bogdan Khmelnytsky National University of Cherkassy
81 Shevchenko Blvd., 18000, Cherkassy, Ukraine

The work presents the results of numerical modeling of thermal fields in the zone of joining aluminium plates through interlayers during local heating of the joint zone by a flat heater, contacting one of the plates. Layers consisting of braze alloy, multilayer reactive foil or layers of both types were considered as an interlayer. Calculation was carried out considering the thermal-physical characteristics of the material of plates, interlayer and heater, consisting of multilayer reactive foils, in which a reaction of self-propagating high-temperature synthesis is accompanied by intensive heat evolution. Conditions of local heating of the aluminium plates necessary for obtaining permanent joints during their brazing or welding through an interlayer were studied. 14 Ref., 1 Table, 11 Figures.

Keywords: *brazing, welding, aluminium alloys, braze alloy, multilayer foil, thermal fields, local heating, permanent joint*

Searching for new approaches for elimination of damage in shell-type structures from aluminium alloys under the conditions of limited access to powerful heat sources is an urgent task, the solution of which will allow increasing structure reliability and operating life [1–3]. From this viewpoint, it appears to be a promising idea to join an aluminium coverplate to the damaged area of the shell surface due to local heating of the joint zone by a heat source ensuring heating of the joint zone up to temperatures, at which conditions are in place, which are needed for joint formation, for instance, melting of a layer of braze alloy, located in the joint zone, or melting of the surfaces being joined.

It is known that reactive materials, which are capable of generating heat during running of the reaction of self-propagating high-temperature synthesis in them (SHS), can be used as the heat source, which in the self-supporting mode can provide the required conditions for welding or brazing of materials [4–6]. At local heating of the joint zone, the heat can be dissipated to the environment and propagate through the structural elements. To ensure heating of the joint zone, it is preferable to use materials with a high rate of heat generation.

As the intensity of heat generation in such materials essentially depends on the rate of SHS reaction running in them, application for these purposes of thermit mixtures seems to be less effective, compared to multilayer foils (MF), consisting of highly reactive materials. In thermit mixtures the rate of SHS reaction propagation is low, because of the small area of contact between the powder components and presence of oxide films on their surface [7]. In the case of MF the reactive layers contact each other over the entire foil surface that ensures the rate of SHS reaction front propagation by 1–2 orders higher, compared to powdered thermit mixtures [8–10]. Such properties of reactive MF allow applying them both as an interlayer for preheating the surfaces of aluminium plates being joined, and as a heater, contacting one of the plates (coverplate), for local heating of the joint zone.

At the same time, in order to apply such an approach to producing permanent joints, it is necessary to take into account the fact that the heat flow, continuously coming from the heater through the coverplate into the joint zone, is removed from it via the second plate (shell). If for instance, a braze alloy interlayer is located in the joint zone, it is important to establish not just the lower power limit of the heater, at which the braze alloy can be melted, but also not exceed the upper limit, at which the coverplate material, contacting the heater, can be surface-melted.

It is clear that heat propagation in such systems is influenced both by thermophysical properties of the material of system elements, and heat transfer (thermal resistances) on the boundaries between them. Here, the thermophysical parameters are usually known, whereas the parameters of heat transfer between the system elements significantly depend on a number of factors (surface roughness, force of their

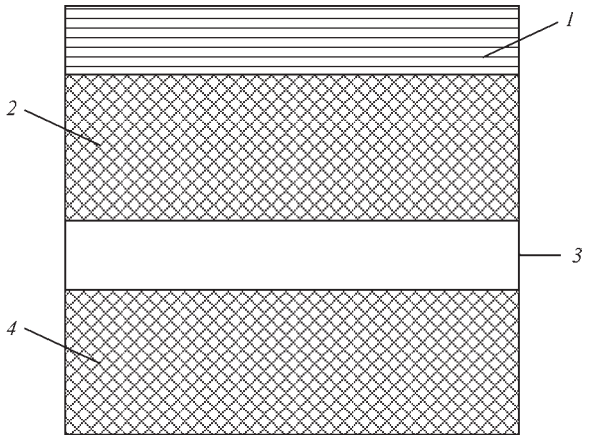

Figure 1. Scheme of joining plates at their heating as a result of contact of coverplate with heater: *1* — heater; *2* — coverplate; *3* — interlayer, *4* — shell in the form of plate

pressing to each other, etc.), which can vary in a broad range. Therefore, it is difficult to perform calculation of thermal fields in such systems in the general case. Earlier conducted investigations of temperature fields under the conditions of nonideal contacts between the system elements, showed [11] that the time of heat redistribution under such conditions is significantly longer. However, general regularities of the change of temperature fields are similar.

In this connection, it was assumed that contacts between the system elements are ideal, in order to clarify the effect of thermophysical characteristics of the studied system materials on thermal fields during joining of aluminium plates through interlayers based on the layers of braze alloy or multilayer highly reactive foil. This allowed clarifying the maximum permissible values of the parameters of the heater with a high rate of heat generation, providing the thermal conditions for producing permanent joints of aluminium plates.

Method of calculation of thermal fields. Scheme of joining plates through an interlayer by local heating of the joint zone through contact of the heater with one of the plates (furtheron referred to as coverplate), is shown in Figure 1. If heater *1*, for instance, of 0.05×0.05 m^2 size, consists of a pack of MF based on Ni and Al layers with equiatomic ratio of elements, characterized by a high rate of running of synthesis reaction, of the order of 1–3 m/s [8], ensuring its heating up to a certain (adiabatic) temperature, characteristic of MF chemical composition and structure over a short time of the order of 0.005–0.015 s, then the time of heater heating up to maximum temperature can be neglected.

Analysis of thermal fields was performed, proceeding from the fact that in the joint zone heating of the surfaces being joined should reach a temperature, which enables running of the processes, required for formation of a permanent joint between these surfaces. So, for joining plates by brazing, the temperature in the contact zone should be higher than the braze alloy melting temperature, and in the case of welding, it should be higher than the melting temperature of plate material.

Analysis of thermal fields was performed in the case of joining aluminium plates from AMg6 alloy. Considered as the heat source, is a pack consisting of MF based on Ni and Al layers with equiatomic element ratio. Similar MF were considered as interlayers for local heating of the joint zone. Used as the braze alloy was a model alloy of eutectic composition with melting temperature of 850 K. Thermophysical characteristics of materials in the system of «heater–coverplate (1st plate)–interlayer-2nd plate (shell)» are shown in the Table.

At modeling the thermal fields in aluminium plate joint zone, layers of braze alloy, MF and presence of layers of both types were considered as interlayers. If we assume that all the system elements have an unlimited size along two coordinates, parallel to the joint plane and limited size in the normal direction, it allows analyzing heat redistribution only in one direction, namely normal to the contact plane.

Characteristics of materials of «heater–coverplate–interlayer–shell» system

Parameters. Properties	Material			
	Multilayer foil Ni/Al (heater)	Aluminium alloy AMg6 (coverplate and 2nd plate (shell))	Model braze alloy (interlayer)	Multilayer foil Ni/Al (interlayer)
Thickness, mm	1–16	5–17	0.1	0.05–0.35
Specific weight, kg/m^3	5164	2650	2650	5164
Heat conductivity, W/m·K	51	126	155	51
Adiabatic temperature of SHS reaction, K	1912	–	–	1912
Braze alloy melting temperature, K	–	–	850	–
Latent heat of melting, kJ/kg	–	400	555	–
Heat of intermetallic formation, eV	0.46	–	–	0.46
Period of layer modulation in multilayer foil, nm	100	–	–	100
Multilayer foil thickness, μm	200	–	–	50–350
Energy of activation of interdiffusion between Al and Ni layers, eV	1.69	–	–	1.69

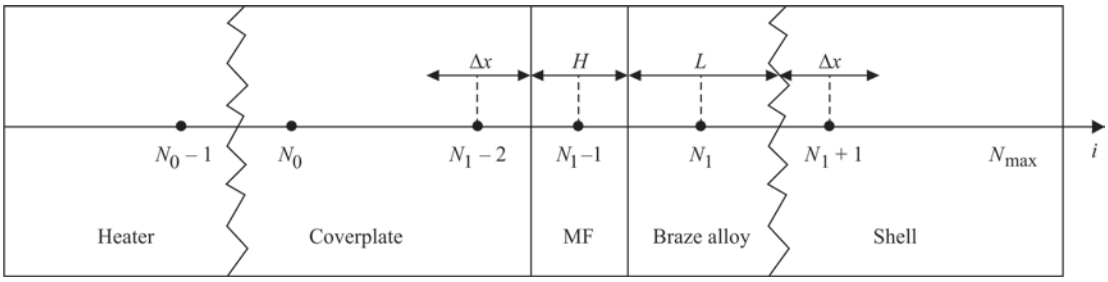

Figure 2. Scheme of division of «heater–coverplate–interlayer–shell» system into cells

All the system elements were divided into cells of a finite thickness Δx, except for the interlayer, which was regarded as one cell of thickness L, in the case of an interlayer based on braze alloy, or thickness H — for reactive MF, and two cells of thickness $L + H$, if the interlayer consists of a layer of braze alloy and MF. All the calculations were performed at system division into cells of 200 μm thickness. Cell numbering is shown in Figure 2.

Assuming that thermal energy radiation outside the system is absent, boundary conditions of the second kind will be satisfied for the extreme cells:

$$T_0 = T_1,\ T_{N_{\max}} = T_{N_{\max}-1}.$$

where $N_{\max}$ is the maximum cell number:

$$N_{\max} = L_0/\Delta x + L_1/\Delta x + L_2/\Delta x + 2,$$

where L_0 is the heater thickness; L_1 is the coverplate thickness; L_2 is the shell thickness.

To determine the temperature in each shell, it is necessary to solve the equation of heat conductivity

$$\frac{\partial T}{\partial t} = a\frac{\partial^2 T}{\partial x^2} \qquad (1)$$

allowing for thermophysical properties of cell materials, where a is the thermal diffusivity of cell material.

Equation of heat conductivity (1) has a solution for all the system cells of width Δx:

$$T_i = T_i^{\text{old}} + a\frac{T_{i+1}^{\text{old}} - 2T_i^{\text{old}} + T_{i-1}^{\text{old}}}{\Delta x^2}dt, \qquad (2)$$

where T_i is the temperature of the i-th cell, which it reaches within dt seconds, compared to initial temperature T_i^{old}. This ratio is valid for all the cells, except for $N_0 = 1$, N_0, $N_1 - 2$; N_1 and $N_1 + 1$, which belong to different system elements. In order to determine the temperature in the cells on the contact boundary, it was assumed that the heat flow is proportional to temperature difference in boundary cells i and $i + 1$, heat transfer between which is characterized by effective «coefficient of heat transfer» $\mu_{i,j+1}$, in keeping with relationship

$$J_{i,i+1} = -\mu_{i,i+1}(T_{i+1} - T_i).$$

In the case of an ideal thermal contact between cells i and $i + 1$, belonging to different system elements with coefficients of heat conductivity of their material k_i and k_{i+1}, thickness h_i and h_{i+1} respectively, the coefficient of heat transfer is defined as

$$\mu_{i,i+1} = \frac{2k_i k_{i+1}}{k_i h_{i+1} + k_{i+1} h_i}. \qquad (3)$$

Then, equation (2) for determination of temperature in boundary cells can be found from the system of equations, which take into account the heat flows between the boundary and adjacent cells.

$$\frac{dT_i}{dt} = \frac{1}{c_i\rho_i}\left(J_{i-1,i} - J_{i,i+1}\right),$$
$$\frac{dT_{i+1}}{dt} = \frac{1}{c_{i+1}\rho_{i+1}}\left(J_{i,i+1} - J_{i+1,i+2}\right), \qquad (4)$$

where c_1 and ρ_i is the heat capacity and specific weight of the material of i-th cell.

As the heat source can have a temperature, which exceeds the melting temperature (T^{melt}) of coverplate material, the possibility of its partial or complete melting should be taken into account. Let at partial melting of the plate the boundary between the liquid and solid phases be located in point $\xi(x_N < \xi < x_{N+1})$ (Figure 3). Then temperature distribution to the left and right of the boundary can be calculated from the balance of heat flows, allowing for the fact that during time dt the boundary will shift by value dy.

$$J_l^Q S dt - J_s^Q S dt = \lambda\rho_{pl1} S dy, \qquad (5)$$

where λ_{pl1}, λ_{pl2}, ρ_{pl1}, ρ_{pl2} are the specific heat of melting and density of plate material; S is the cross-sectional area; dy is the change of the boundary position.

Allowing for the coefficients of heat transfer in the liquid (l) and solid (s) phases, equation (5) can be written as

$$\frac{dy}{dt} = \frac{J_l^Q - J_s^Q}{\lambda\rho_{pl1}} = \frac{\kappa_1^l\left.\frac{\partial T}{\partial x}\right|^l + \kappa_1^s\left.\frac{\partial T}{\partial x}\right|^s}{\lambda\rho_{pl1}}. \qquad (6)$$

Then the change of temperature of cells N' and $N' + 1$ during time dt can be calculated, proceeding from equations

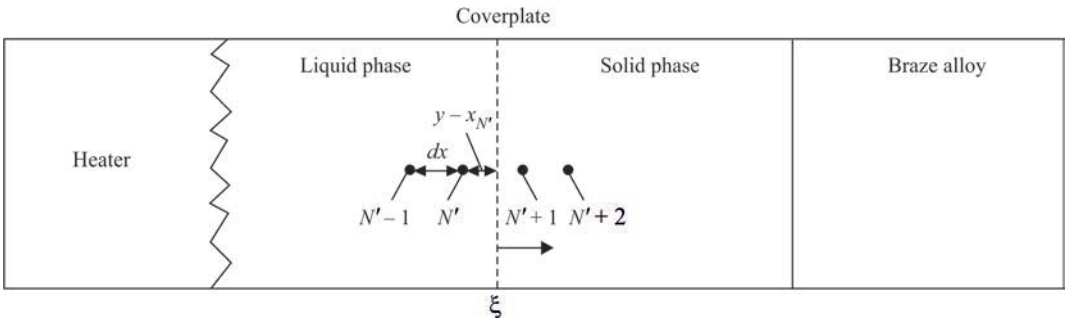

Figure 3. Schematic image of the interface of the liquid and solid parts of the plate during its melting

$$\frac{T_{N'}^{\text{new}} - T_{N'}^{\text{old}}}{dt} = a_{\text{pl1}}^{\text{l}} \frac{\dfrac{T^{\text{melt}} - T_{N'}}{\xi - x_{N'}} - \dfrac{T_{N'} - T_{N'-1}}{dx}}{\dfrac{(\xi - x_{N'-1})}{2}}, \quad (7)$$

$$\frac{T_{N'+1}^{\text{new}} - T_{N'+1}^{\text{old}}}{dt} = a_{\text{pl1}}^{\text{l}} \frac{\dfrac{T_{N'+2} - T_{N'+1}}{dx} - \dfrac{T_{N'+1} - T^{\text{melt}}}{x_{N'+1} - \xi}}{\dfrac{(x_{N'+2} - \xi)}{2}}. \quad (8)$$

Such calculations should be performed at each time step, simultaneously following the position of the boundary. We will calculate the new position of the boundary of the liquid and solid phases from the following formula:

$$\xi^{\text{new}} = \xi + \frac{dt}{\lambda \rho_{\text{pl1}}} \times \left(\kappa_1^{\text{s}} \frac{T_{N'+1} - T^{\text{melt}}}{x_{N'+1} - \xi} - \kappa_1^{\text{l}} \frac{T^{\text{melt}} - T_{N'}}{\xi - x_{N'}} \right), \quad (9)$$

Temperature of plate cells, which are located to the left and right from the interface (except for near-boundary layers) is calculated by formula (4), but with different heat conductivity: κ_1^{l} for the molten part and κ_1^{s} for the solid part of the plate.

In the case, when the braze alloy, located in the gap between the plates, is partially melted, the equations for temperature calculations in the adjacent cells will be similar (5)–(9), just the heat conductivity κ_1^{s} inherent to the solid phase of the braze alloy, should be changed to the heat conductivity κ_1^{l} of the liquid phase.

At partial melting of the braze alloy, the position of liquid-solid phase boundary can be described by parameters η ($0 < \eta < 1$), as shown in Figure 4.

Heat losses/contribution at melting/solidification can be allowed for from the difference in the heat flows. Heat change can be recalculated to the fraction of the melt in the vicinity of the plate cell

$$\left(J_{\text{in}}^{Q} - J_{\text{out}}^{Q}\right) dt = S \rho_{\text{br}} \lambda_{\text{br}} L d\eta, \quad (10)$$

where λ_{br} is the specific heat of melting of braze alloy; ρ_{br} is the braze alloy density; S is the cross-sectional area; L is the thickness of braze alloy layer; $d\eta$ is the change of molten braze alloy fraction; J_{in}^{Q}, J_{out}^{Q} are the heat flows entering and leaving the molten braze alloy, respectively.

Magnitude of heat flows on the boundaries between the cell contacting the molten braze alloy and the braze alloy, and the one between the braze alloy in the solid phase and adjacent cell of the shell can be written as

$$J_{\text{in}}^{Q} = -S \kappa_1^{\text{s}} \frac{T_x - T_{N_1}}{dx/2}, \quad (11)$$

$$J_{\text{out}}^{Q} = -S \mu_1 \left(T_{N_{2+1}} - T_{evt} \right). \quad (12)$$

where T_{evt} is the braze alloy melting temperature.

Temperature value on the boundary between the plate and the melt can be determined from the equality of heat flows from the plate into the braze alloy melt and from the melt into the solid phase of braze alloy

$$-\kappa_1^{\text{s}} \frac{\left(T_x - T_{N_1}\right)}{dx/2} = -\kappa_1^{\text{l}} \frac{\left(T_{evt} - T_x\right)}{\eta L}. \quad (13)$$

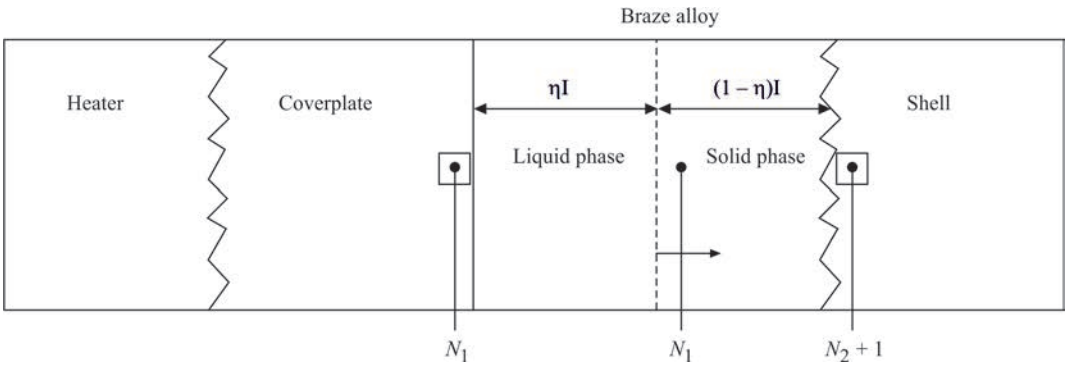

Figure 4. Schematic image of the position of the interface between the liquid and solid phase of braze alloy at its partial melting η

Change of the position of the boundary of braze alloy melt during time dt can be calculated from equation

$$\eta_i^{\text{new}} = \eta_i + \frac{dt}{\rho_{\text{br}}\lambda_{\text{br}}L}\times$$
$$\times\left(\frac{2\kappa_1^{\text{s}}\kappa_1^{\text{l}}}{2\kappa_1^{\text{s}}\eta L + \kappa_1^{\text{l}}dx}(T_{N_1} - T_{evt}) + \mu_1(T_{N_2+1} - T_{evt})\right). \quad (14)$$

Change of temperature on the boundaries with the plates, allowing for partial melting or solidification of the braze alloy, can be calculated from the following expressions:

$$T_{N_1}^{\text{new}} = T_{N_1} + \frac{dt}{dx\rho_{\text{pl1}}c_{\text{pl1}}}\times$$
$$\times\left(-\frac{\kappa_1^{\text{s}}}{dx}(T_{N_1} - T_{N_1-1}) + \frac{2\kappa_1^{\text{s}}\kappa_1^{\text{l}}}{\kappa_1^{\text{s}}\eta L + \kappa_1^{\text{l}}dx}(T_{N_1+1} - T_{N_1})\right), \quad (15)$$

$$T_{N_2+1}^{\text{new}} = T_{N_2+1} + \frac{dt}{dx\rho_{\text{pl2}}c_{\text{pl2}}}\times$$
$$\times\left(\mu_1(T_{evt} - T_{N_2+1}) + \frac{\kappa_1^{\text{l}}}{dx}(T_{N_2+2} - T_{N_2+1})\right). \quad (16)$$

If the composition of the interlayer includes MF based on reactive elements, then during heating the diffusion processes between the reactive element layers will be initiated in the foil, leading to formation of intermetallic compounds. As this process will be accompanied by heat evolution, cells contacting the foil will be heated by heat flow not only from the heater, but also from MF.

Using Wagner coefficient of diffusion [12] and the law of phase growth at reaction diffusion [13], it is possible to determine the thickness of the interlayer of intermetallic phase, which forms on the boundary of reactive element layers, $d\Delta y$ during time interval dt, as

$$d\Delta y = \frac{D_0\Delta g}{k_B T_{N_1} c(1-c)}\exp\left(-\frac{Q}{k_B T_{N_1}}\right)dt,$$

where T_{N_1} is the temperature of the interlayer with a multilayer structure at the initial moment of time.

Change of temperature in the foil cell as a result of such a phase transformation is determined as

$$T_{N_1} = T_{N_1} + \frac{d\Delta y}{2l}\frac{\Delta g}{3k_B}.$$

where Δg is the heat of formation of the intermetallic phase during the reaction of synthesis in the multilayer structure with modulation period $2l$. Here, it is necessary to take into account the fact that the process of heat generation starts at the thickness of new phase interlayer $\Delta y = \Delta y0$ and goes on up to complete transformation of MF into intermetallics.

If the interlayer composition includes a layer of braze alloy, the calculation took into account absorption of thermal energy in this layer, which is consumed for its heating and melting.

Such a scheme of calculation of the thermal field in the system can be defined both as spatial distribution of temperature, and as its change in a specified point, depending on the time of local heating process.

Within this scheme, temperature distributions when producing permanent joints of aluminium plates by brazing or welding were studied under the condition that the zone of contact of heater with the coverplate and of the coverplate with the shell has contact points, and the coefficients of heat transfer between them are described by relationship (3).

Calculation results. Temperature variation in the interlayer, consisting of a layer of braze alloy during local heating of the joint zone is shown in Figure 5.

One can see that the heater thickness influences the features of temperature variation in the interlayer: at heater thickness below a certain critical value (at selected parameters of the system this corresponds to heater thickness of 5 mm), the temperature in the interlayer increases monotonically. It, however, does not reach braze alloy melting temperature, and at

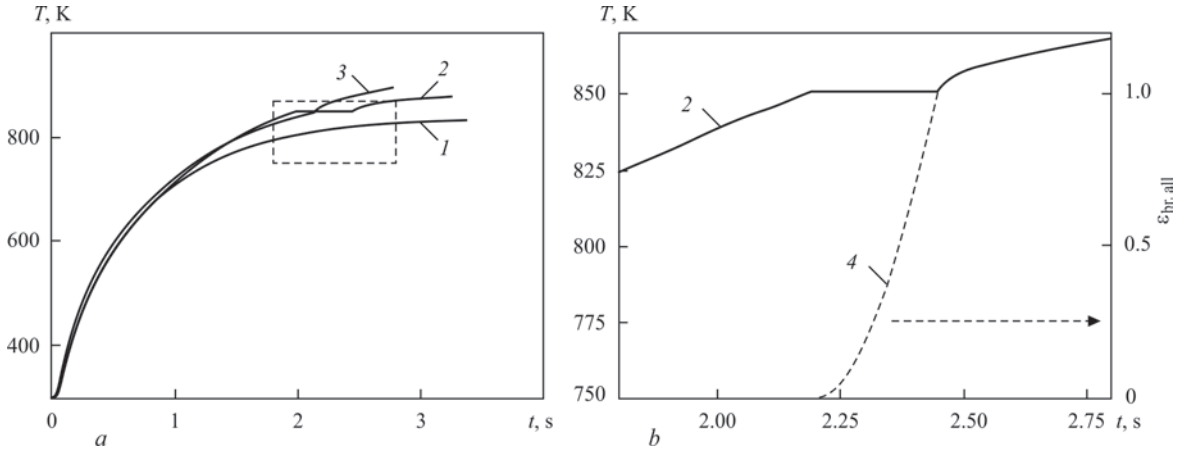

Figure 5. Temperature changes in 100 μm thick interlayer based on «eutectic alloy» (melting temperature of 850 K), depending on thickness of heater with adiabatic temperature of SHS reaction of 1600 K: *1* — d = 5; *2* — 6; *3* — 7 mm (*a*); the insert shows the dependence of melt volume fraction ε_{br} in braze alloy interlayer (curve *4*) during local heating of the joint zone for curve *2* (*b*)

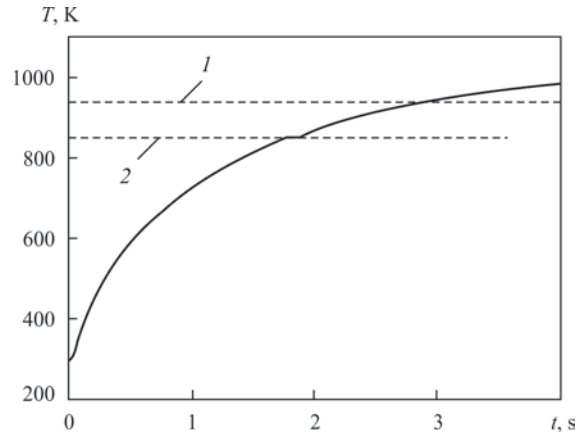

Figure 6. Change of temperature in 100 μm interlayer based on «eutectic alloy» (melting temperature of 850 K) at local heating of plates by 9 mm thick heater (heater adiabatic temperature of 1600 K): *1* — melting temperature of aluminium plates; *2* — braze alloy melting temperature

thickness greater than the critical one (6 mm) a section of slow temperature rise is observed on the temperature dependence. One can see in Figure 5 that this «site» on the temperature dependence corresponds to braze alloy melting. Volume fraction of molten braze alloy becomes larger during soaking at this temperature. Further temperature rise in the interlayer is observed only after complete melting of the braze alloy.

Proceeding from that, it can be assumed that to ensure the temperature mode of brazing the heater thickness should exceed a certain lower limit. However, if a thicker heater were to be used, for instance, 9 mm thick, the temperature in the contact zone after complete melting of the braze alloy will continue rising right up to melting temperature of the aluminium alloy (Figure 6). This results in partial melting of the coverplate, contacting the heater.

Thus, in order to ensure the conditions, required for brazing, the heater thickness should be between the lower and upper limits, that allows melting the braze alloy without leading to coverplate melting.

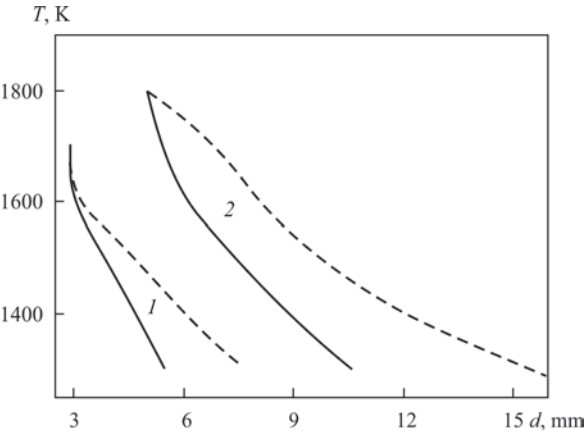

Figure 7. Dependence of lower (solid line) and upper (dotted line) values of heater thickness limits on its adiabatic temperature: *1* — optimum thickness of heater for joining 5 mm aluminium plates; *2* — 10 mm

As the intensity of the heat flow propagating from the heater to the coverplate, depends not only on heater thickness, but also on adiabatic temperature, which it reaches as a result of SHS reaction passing in it, the values of the lower and upper limits of heater thickness were determined in the work, depending on its temperature in the range of 1300–1600 K. Here, the lower limit corresponds to the condition, at which braze alloy melting proceeds without surface melting of the coverplate layers, contacting the heater, and the upper limit corresponds to the conditions of partial (up to 10 %) melting of the coverplate.

One can see from Figure 7 that with increase of adiabatic temperature of the heater, the values of lower and upper limits of its thickness become smaller, as does the difference between these limits. At heater temperature above 1600 K, partial melting of the coverplate is observed already at thicknesses below the lower limit.

Based on that we can conclude that there exist certain limitations, not only for selection of heater thickness, but also for adiabatic temperature, which it reaches as a result of SHS reaction running in it.

Temperature distribution across the cross-section of the assembly at different stages of its heating is shown in Figure 8 for the case of application of the heater, satisfying the above requirements. One can see that for such heaters at all the stages of local heating of the joint zone, the temperature in the contact zone of the heater and coverplate remains practically unchanged, and its value is below the melting temperature of plate material (AMg6 alloy).

A qualitatively new kind of temperature variation is observed in the case, when the interlayer consists of MF based on reactive elements. As one can see from Figure 9, at heating of such an interlayer the nature of its temperature variation depends on heater thickness. A heater thickness of the order of 1 mm, interlayer heating proceeds monotonically. At increase of

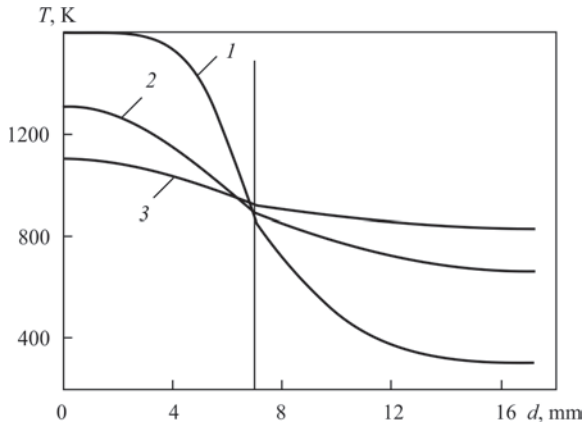

Figure 8. Temperature distribution in the cross-section of the assembly, consisting of 7 mm thick heater, 5 mm coverplate; 100 μm interlayer and 5 mm second plate at different stages of the brazing process: *1* — 0.1 of the process; *2* — 1; *3* — 1.9 s

heater thickness an abrupt increase of temperature is observed on temperature dependence, which after reaching a certain peak value decreases to the level of monotonic dependence, similar to the one characteristic for local heating of the plates in the case of application of interlayers based on braze alloy.

According to work [14], such an abrupt temperature rise in the interlayer with a multilayer structure based on reactive elements can be related to initiation of thermal explosion reaction (TE) in the foil, at which the process of high-temperature synthesis runs in its entire volume without any additional heat input. There exists a threshold value of MF heating temperature for TE initiation: at MF heating rates below the threshold value, the synthesis reaction develops in the mode of solid-phase reaction, requiring continuous heat input, and at higher heating rates the heat generated through high-temperature synthesis, ensures running of this reaction without any external heat input. Therefore, at low heating rates, which are realized in the case of application of 1 mm thick heater, TE is not initiated, whereas at increase of the heating rate due to the heater 1.5 mm thick TE is initiated, which is accompanied by an abrupt increase of temperature in the joint zone. At further increase of MF heating rate due to increase of heater thickness, the value of temperature peak increases, whereas the time of its initiation shifts closer to the start of the heating process.

Ability to heat the joint zone of aluminium plates due to the heat, released in MF at TE, was studied from the viewpoint of creation of thermal conditions for surface melting of aluminium layers, contacting MF that is a mandatory condition for fusion welding. Figure 10 shows temperature distribution in the assembly cross-section at the moment of initiation of synthesis reaction in TE mode in MF. One can see that with increase of MF thickness the temperature in the joint zone rises at TE initiation. Here, a considerable temperature rise is observed in the interlayer and sections of the joined plates contacting MF. At more than 200 μm thickness of the interlayer, the temperature of aluminium alloy layers contacting MF, becomes higher than its melting temperature. It can be assumed that such temperature conditions on the boundary of MF and aluminium plate can promote melting of its surface layers.

Therefore, at application of MF as interlayer, additional heating of aluminium plate layers contacting MF can be provided, as a result of initiation of synthesis reaction in TE mode in it. Owing to increase of MF layer thickness, the quantity of heat generated here, can provide surface melting of aluminium plates, required for their welding.

Note that for the welding mode the heater thickness can be significantly smaller than in the case of

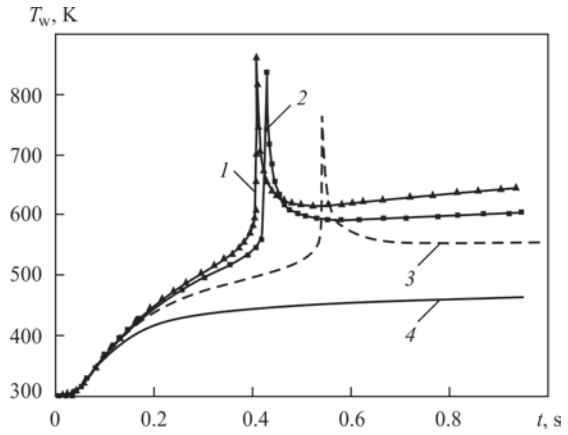

Figure 9. Changes of temperature in the interlayer from MF based on Ni/Al (200 μm thickness with 100 nm period), depending on the time of reaction running at different heater thicknesses: *1* — *d* = 2.5; 2 — 2; *3* — 1.5; *4* — 1 mm, heated up to the temperature of 1600 K

joining plates in the brazing mode. Proceeding from that the possibility of TE application to ensure the thermal conditions required for brazing in the case of application of layers of braze alloy and MF as interlayer, was considered.

Figure 11 shows temperature distribution in the cross-section of an assembly, consisting of a layer of MF and layer based on braze alloy, at the moment of TE initiation. One can see that as a result of TE, the temperature in the interlayer increases abruptly up to values, exceeding the braze alloy melting temperature. Proceeding from that, it can be assumed that such an interlayer structure allows reducing the heater thickness, compared with the process of brazing through the interlayer based on braze alloy, and, consequently, lowering the temperature to which the assembly as a whole will be heated.

The above parameters, characterizing the heater, and their connection with interlayer parameters and thickness of the joined plates, were obtained for the

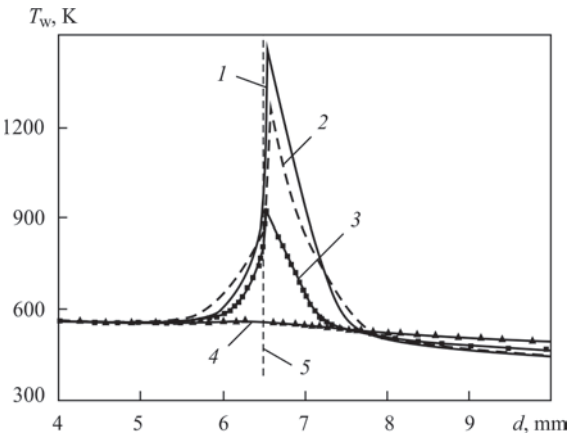

Figure 10. Temperature distribution in the cross-section of an assembly, consisting of heater, coverplate, interlayer based on MF and shell, at the moment of TE initiation in it (heater thickness of 1.5 mm) with different MF thickness: *1* — *df* = 350; *2* — 300; *3* — 200; *4* — 100 μm; *5* — zone between coverplate and MF

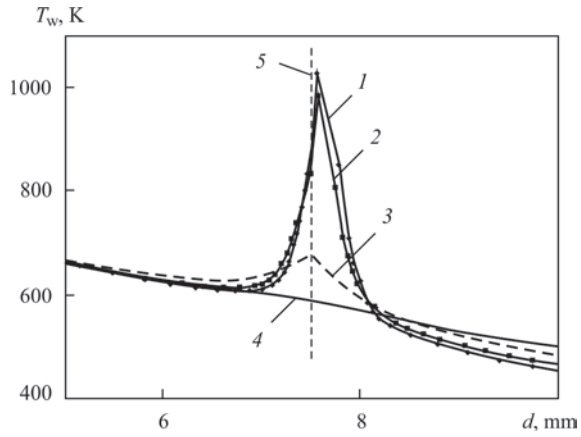

Figure 11. Temperature distribution in the cross-section of an assembly, consisting of heater, coverplate, interlayer based on MF, braze alloy layer (100 μm thickness of braze alloy) and shell, at the moment of TE initiation in MF (heater thickness of 2.5 mm) at different MF thickness: *1* — *df* = 200; *2* — 150; *3* — 100; *4* — 50 μm; *5* — zone between coverplate and MF

case of joining 5 mm thick plates. To clarify the applicability of this approach for joining thicker plates, the temperature fields were calculated in the work, which are required for realization of such a joining scheme. It turned out that the main regularities of local heating of the joint zone using the heater, contacting the coverplate, are preserved under the condition of increasing the heater thickness in proportion to increase of the thickness of the plates being joined, right up to 20 mm.

Conclusions

1. It is shown that at local heating of the zone of the joint of aluminium alloy plates from AMg6 alloy up to 20 mm thick, by a heater based on MF, contacting one of them (coverplate), temperature conditions can be provided, which are required for melting the braze alloy located in the joint zone without melting the aluminium plate.

2. To ensure the temperature conditions, required for the process of brazing the aluminium plates through an interlayer based on braze alloy, at local heating of the joint zone by a heater contacting one of the plates, its thickness should be greater than a certain critical value, dependent on adiabatic temperature of the heater, characteristics of the interlayer based on the braze alloy and plate thickness.

3. It is shown that there exists an upper limit of adiabatic temperature of the heater, above which melting of the coverplate material can occur earlier, than melting of the braze alloy layer, located in the joint zone.

4. Application of multilayer foil as interlayer, for instance, Ni/Al, which is highly reactive, can ensure the temperature conditions for running of the welding process due to local melting of aluminium alloy layers contacting the interlayer, as a result of initiation of synthesis reaction in the foil by the scheme of thermal explosion (bulk synthesis reaction) at local heating of the joint zone by the heater, contacting the coverplate.

5. Application of an interlayer from highly reactive multilayer foil, for instance, Ni/Al, in combination with a layer of braze alloy, allows reducing the thickness of the heater, required to provide the temperature conditions for the brazing process due to additional heat generation in MF at initiation of high-temperature synthesis in it in thermal explosion mode.

1. Ishchenko, A.Ya. (2004) Specifics in application of aluminium high-strength alloys for welded structures. *The Paton Welding J*., **9**, 15–25.
2. Krivtsun, I.V., Kvasnytsky, V.V., Maksymov, S.Yu., Ermolaev, G.V. (2017) *Special methods of welding*. Ed. by B.E. Paton. Mykolaiv, NUK [in Ukrainian].
3. Ishchenko, A.Ya. (2002) Investigation and development of the technology of light alloy welding at the PWI. *The Paton Welding J*., **12**, 25–26.
4. Subramanian, J.S., Rodgers, P., Newson, J. (2005) Room temperature soldering of microelectronic components for enhanced thermal performance. In: *Proc. of 6th. Int. Conf. on Thermal, Mechanical and Multiphysics Simulation and Experiments in Micro-Electronics and Micro-Systems «EuroSimE»*. Berlin, 681–686.
5. Ramos, A.S., Vieira, M.T., Simões, S. et al. (2010) Reaction-assisted diffusion bonding of advanced materials. *Defect and Diffusion Forum*. **297–301**, 972–977.
6. Weihs, T., Barmak, K., Coffey, K. (2014) Fabrication and characterization of reactive multilayer films and foils. *Metallic Films for Electronic, Optical and Magnetic Applications: Structure, Processing and Properties*, **40**, 160–243.
7. Seshadri, R. (2000) Centrifugal casting of metals and ceramics using thermite reactions. *Metals Materials and Processes*, **12**, 233–240.
8. Kravtchuk, M.V., Ustinov, A.I. (2015) Influence of thermodynamic and structural parameters of multilayer foils on SHS process characteristics. *The Paton Welding J*., **8**, 8–13.
9. Knepper, R., Snyder, M., Fritz, G. et al. (2009) Effect of varying bilayer spacing distribution on reaction heat and velocity in reactive Al/Ni multilayers. *J. of Applied Physics*, **105**, 083504-1–083504-9.
10. Zaporozhets, T.V., Gusak, A.M., Ustinov, A.I. (2010) Modeling of stationary mode of SHS reaction in nanolayer materials (phenomenological model). 1. Single-stage reaction. *Sovrem. Elektrometall*., **1**, 40–46 [in Russian].
11. Kulinich, M.V., Bezpalchuk, V.M., Kosintsev, S.G. et al. (2018) Calculation-experimental investigation of thermal fields in the process of nonstationary soldering. *The Paton Welding J*., **1**, 14–19.
12. Zaporozhets, T.V., Korol, Ya.D. (2016) Approach of inverse problem for prediction of characteristics of self-propagating high-temperature synthesis in multilayer foils taking into account competitive phase formation. *Metallofiz. i Novejshie Tekhnologii*, 38(**11**), 1541–1560 [in Russian].
13. Umansky, Ya.S., Finkelshtejn, B.N. et al. (1958) *Physical metals science*. Moscow, Metallurgizdat [in Russian].
14. Ustinov, A.I., Kuzmenko, D.N., Kravchuk, M.V., Korol, Ya.D. (2015) Initiation of thermal explosion in Ti/Al nanofoils. *Int. J. of SHS*, 24(**2**), 72–77.

Received 06.02.2019

DOI: http://dx.doi.org/10.15407/tpwj2019.04.04

APPLICATION OF ULTRAFINE NICKEL POWDER FOR DIFFUSION JOINING OF TITANIUM TO STAINLESS STEEL

A.V. LYUSHINSKY
JSC «Ramenskoje Instrument Design Bureau»
2 Gurieva Str., 140103, Ramenskoje, RF. E-mail: nilsvarka@yandex.ru

The paper deals with the features of joining titanium alloy PT-3V to steel 08Kh18N10T by diffusion welding with application of an interlayer of ultrafine nickel powder, produced by thermal decomposition of nickel formate $Ni(COOH)_2$ + + $2H_2O$. Comparison of the structures of welded joints of these materials for presence of intermetallic phases in welding without interlayers and with a nickel interlayer at different mode parameters was performed. Application of ultrafine nickel powder at temperatures of 965 and 890 °C leads to formation of a continuous layer of solid intermetallics. At the temperature of 790 °C the diffusion zone has a multilayer structure, differing from the microstructure of steel-titanium joint, produced without the nickel interlayer. Mechanical rupture testing of the welded joints showed that sufficient strength properties are achieved at application of an interlayer of ultrafine nickel powder at lower temperature and pressure, preventing intensive growth of intermetallics. The highest values of ultimate strength were achieved at welding temperature of 760–790 °C and were equal to 346 MPa on average. 13 Ref., 3 Tables, 4 Figures.

Keywords: *diffusion welding, interlayer, ultrafine powder*

An urgent task for industry always is joining parts and assembly units, manufactured from dissimilar materials, into serviceable components, for instance of «α-titanium alloy + stainless steel 08Kh18N10T» combination by diffusion welding method. It is known [1–4] that joining titanium alloys to alloys containing nickel, involves certain difficulties [5–7] because of formation of intermetallics between these two elements [8]. It is understandable that in order to achieve the required service properties of welded joints, diffusion welding should be conducted under the conditions, limiting formation of intermetallic phases in the diffusion zone of the welds. In other words, the welding process should be realized at temperatures below those of the start of intermetallic formation [9–11]. Naturally, there arises the need for application of interlayers, and not just for elimination of formation of intermetallics in the joint zone, but also for lowering the welding temperature and pressure, this way not promoting their growth. Such an ambiguous task can be solved with application of interlayers in the form of highly-reactive high-energy powder materials, providing:

- considerable lowering of thermodeformational impact on the materials being welded;
- intensification of running of diffusion processes at abruptly lowered temperatures;
- preservation of initial properties of these materials;
- sufficient mechanical strength of welded joints of dissimilar materials [11–13].

In welding of dissimilar metals and alloys nickel is often used as interlayer that is due to its favourable physicochemical properties and good metallurgical compatibility with the majority of metals [3–7]. Investigations of diffusion welding with application of interlayers from various nickel powders with different dispersity: d — electrolytical (PNE-1, d = 39.75 μm), carbonyl (PNKOT-1, d = 7.63 μm) and ultrafine, produced by thermal decomposition of nickel formate $Ni(COOH)_2 + 2H_2O$ (d < 0.01 μm) showed that maximum strength is achieved in welding through ultrafine powder (UFP) [7, 11, 13]. This powder has minimum particle size, and the size of specific surface can be regulated at pyrolysis of nickel formic acid and can reach 20 m^2/g. A greater value can be also achieved, but UFP becomes pyrophoric and, naturally, difficult to work with. Moreover, this UFP features purity of the product and absence of impurities.

Application of nickel UFP allows lowering welding temperature to values, partially or completely eliminating formation of brittle intermetallic inclusions or liquid eutectics between the materials being joined. This factor is responsible for producing diffusion joints with high mechanical properties [3–5, 7, 11].

The paper gives the results of experimental studies on optimization of the technology of diffusion welding of austenitic steel 08Kh18N10T to titanium alloy PT-3V through an interlayer of nickel UFP and presents the results of metallographic examination of welded joints and mechanical tensile testing of welded samples. Tables 1, 2 give the chemical composition of the studied materials.

The main objective of the work was producing diffusion welded joints with high stable mechanical properties without inadmissible internal defects while ensuring lowering of the joining process temperature.

Table 1. Chemical composition of alloy PT-3V, wt.%

Elements	Ti	Fe	V	Al	Zr	Si	C	N	Res.
Content	91.39–95.0	up to 0.25	1.2–2.5	3.5–5.0	up to 0.3	up to 0.12	up to 0.1	up to 0.4	0.45

Table 2. Chemical composition of 08Kh18N10T, wt.%

Elements	Ti	Fe	Cu	Cr	P	S	Ni	Mn	Si
Content	0.4–1.0	67	up to 0.3	17–19	up to 0.035	up to 0.02	9–11	up to 2	up to 0.8

Used as an interlayer was nickel UFP, rolled into a strip 60 μm thick with 55 % porosity. Size of particles of initial nickel UFP (main fraction) is less than 0.01 μm, specific surface of the powder is about 17 m^2/g. After rolling UFP into a strip only the value of specific surface of the powder changes, but by not more than 8 %. But the strip ensures producing welds of uniform thickness and density, and at the same time allows realizing an extremely large margin of free energy of powder particles, from which it consists [7, 11–13].

Experiments were conducted on cylindrical samples from titanium alloy PT-3V and steel 08Kh18N10T of 20 mm diameter and 30 mm height each. Welding was performed in a diffusion welding unit SDVU-50 with radiation heating, providing vacuum not lower than $5 \cdot 10^{-5}$ mm Hg.

A strip from nickel UFP was placed between the materials being joined.

During experiments, welding temperature T and soaking time t were varied, and welding pressure P = = const = 27.5 MPa.

Produced blank was used to cut out a sample for metallographic examination, which was conducted in Neophot microscope at ×250 magnifications. Then parts for mechanical tensile testing by a standard procedure were cut out of the studied samples.

Authors of works [2, 9] considered the features of phase formation when joining steel 08Kh1810T to PT-3V alloy by diffusion welding directly, without interlayers. Proceeding from studies of the microstructure of this joint (Figure 1), it is shown that the joint zone is characterized by presence of an interlayer of intermetallics formed between titanium and iron at T = 965 °C for 1 min. This mode ensures the strength of the joint of about 255 MPa that is almost by 100 MPa lower than the required value at operation of this component.

In this study analysis of the influence of an interlayer from nickel UFP on the strength of welded joint through growth of intermetallic phases at different temperatures of diffusion welding was performed. Table 3 gives sample numbers, their joining modes and results of rupture testing. Temperature of welding samples No.2 and No.3 corresponded to that of welding sample No.1, as it was necessary to evaluate the influence of nickel UFP layer on welded joint strength. As one can see, in this case the strength is much lower than in welding without the interlayer. In [11] it is shown that this is related to high diffusion activity of nickel UFP. The other experimental temperatures (890 and 790 °C) are taken from critical points of Ni–Ti constitutional diagram, and temperature of 760 °C is the temperature at which no sound joint of alloys PT-3V and 08Kh18N10T without the interlayer can form, and the joint with an interlayer has σ_t = 355 MPa.

Metallographic examination of welded joints produced by diffusion welding of austenitic steel and titanium alloy through a layer of nickel UFP, revealed their multilayer structure (Figure 2). They differ from the microstructure given in Figure 1.

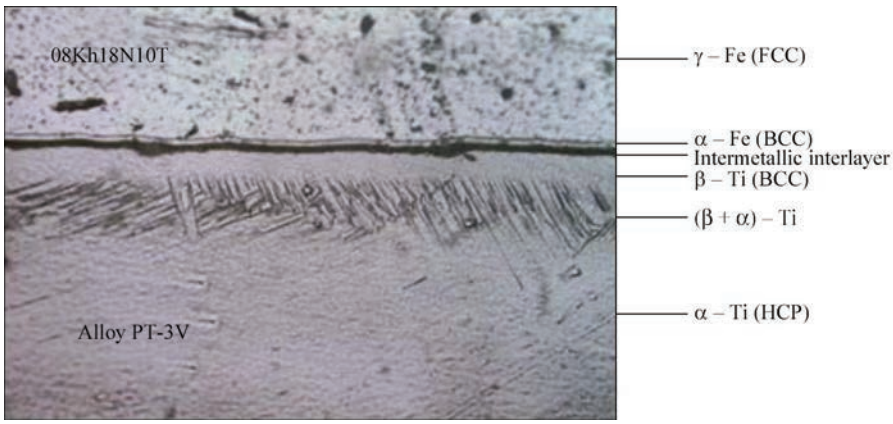

Figure 1. Microstructure (×300) of steel-titanium welded joint, made by diffusion welding in the mode of T = 965 °C, t — 1 min without application of interlayers [2, 9]

Table 3. Samples made by diffusion welding through a layer of nickel UFP and without it

Sample number	Presence of an interlayer	Temperature *T*, °C	Welding time, *t*, min	σ_t, MPa
1	No layer	965	1	255
2	UFP	965	1	150
3	UFP	965	3	140
4	No layer	890	1	250
5	UFP	890	3	53
6	UFP	790	10	349
7	UFP	790	5	311
8	UFP	790	20	311
9	UFP	790	15	307
10	UFP	760	15	355

Welding at 890 °C, 1 min and at 965 °C, 1 min. leads to formation of a phase, which, according to Ti–Ni constitutional diagram, is an intermetallic Ti_2Ni phase (Figure 2, *a*, *b*). Thickness of this phase reached 14 and 22 μm, respectively. Increase of soaking time up to 3 min leads to appearance of eutectic phase Ti_2Ni + + α + β of up to 128 and 152 μm thickness, respectively (Figure 2, *c*, *d*).

Microstructure of the metal of joints produced by welding at 760 and 790 °C with soaking for 5–20 min (Figures 3, 4) has the following features:

• a nickel layer on average 40 μm thick, containing pores, is observed from the steel side;

• α-Fe and β-Ti phases characteristic for diffusion joint of steel with titanium without UFP interlayer, are absent that is indicative of the absence of interdiffusion of elements of steel and titanium alloy through a layer of nickel, i.e. diffusion joint formed over a layer of nickel;

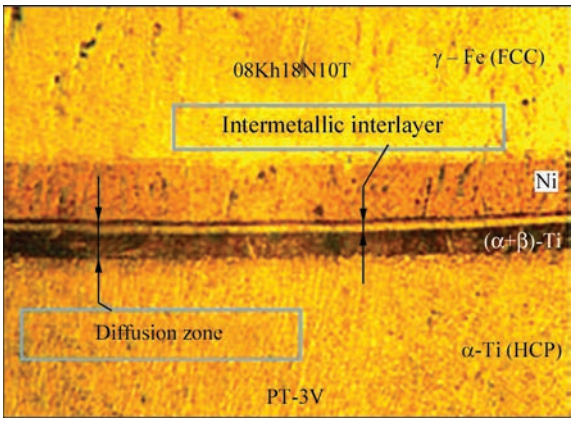

Figure 3. Microstructure of metal (×250) of a welded joint of austenitic steel with titanium alloy, made by diffusion welding at 790 °C, 10 min, through an interlayer from nickel UFP

• a diffusion zone is observed between the nickel layer and titanium alloy, which includes intermetallic phase Ti_2Ni up to 12 μm thick, interdiffusion zone up to 10 μm thick and (α + β)-Ti layer up to 30 μm thick, formed as a result of nickel diffusion into titanium.

One can see from Table 1 that interlayer application at the temperature of 965 and 890 °C was detrimental for welded joint strength, compared to the results of welding without interlayer application. Samples, welded at temperatures of 760–790 °C, have ultimate strength equal to 346 MPa on average. This is attributable to minimum zone of intermetallic inter-

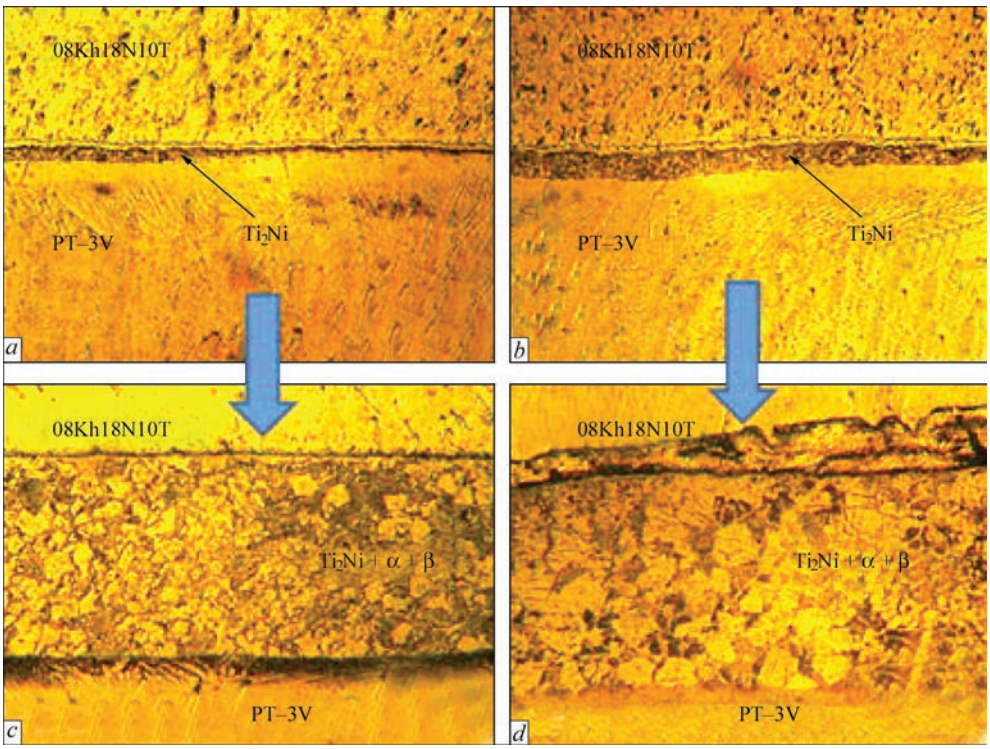

Figure 2. Microstructure of metal (×250) of welded joints made by diffusion welding of austenitic steel to titanium alloy through an interlayer from nickel UFP in the following modes: *a* — 890 °C, 1 min; *b* — 965 °C, 1 min; *c* — 890 °C, 3 min; *d* — 965 °C, 3 min

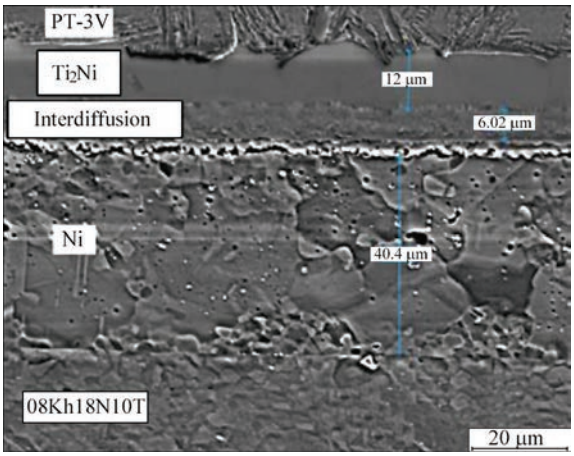

Figure 4. Microstructure of metal in welded joint of austenitic steel with titanium alloy, made by diffusion welding at 760 °C, 15 min through an interlayer from nickel UFP

layer in the welded joint and long-term interdiffusion of the materials being joined.

Conclusions

1. Application of nickel UFP at temperatures of 965 and 890 °C leads to formation of a continuous layer of solid intermetallics. At the temperature of 790 °C the diffusion zone has a multilayer structure, differing from that of steel-titanium joint, produced without the nickel interlayer. A wide nickel layer is observed from the steel side, and a layer of (α + β)-Ti – from the titanium side.

2. Mechanical tensile testing of welded samples showed that the highest values of ultimate strength were achieved at welding temperatures of 760–790 °C, and were equal to 346 MPa on average.

3. Performed work confirms the positive effect from application of highly-reactive nickel UFP in welding titanium to steel. It becomes possible to conduct welding at temperatures of 760–790 °C, avoiding formation of brittle intermetallic phases directly between alloys PT-3V and 08Kh18N10T. Intermetallic layers, formed between the interlayer and titanium alloy at the temperature of 760 °C, have no decisive impact on welded joint strength.

1. Kazakov, N.F. (1976) *Diffusion welding of materials*. Moscow, Mashinostroenie [in Russian].
2. Uvarov, A.A. Semenov, A.N., Krestnikov, N.S. et al. (2017) Examination of structure of steel-titanium welded joints, produced by diffusion welding using ultrafine nickel powders. *Metallovedenie i Termich. Obrab. Metallov*, **8**, 57–61 [in Russian].
3. Kireev, L.S., Zamkov, V.N. (2002) Solid-state joining of titanium to steel (Review). *The Paton Welding J.*, **7**, 29–35.
4. Ustinov, A.I., Falchenko, Yu.V., Melnichenko, T.V. et al. (2015) Vacuum diffusion welding of stainless steel through porous nickel interlayers. *Ibid.*, **7**, 3–9.
5. Bachin, V.A., Kvasnitsky, V.F., Kotelnikov, D.I. et al. (1991) *Theory, technology and equipment for diffusion welding*. Moscow, Mashinostroenie [in Russian].
6. Karakozov, E.S. (1976) *Solid-state joining of metals*. Moscow, Metallurgiya [in Russian].
7. Lyushinsky, A.V. (2006) *Diffusion welding of dissimilar materials*. Moscow, Akademiya [in Russian].
8. Khansen, M., Anderko, K. (1962) *Structures of binary alloys*. Vol. 1, 2. Moscow, Metallurgiya [in Russian].
9. Uvarov, A.A. Semenov, A.N., Novozhilov, S.N. et al. (2014) Technology of manufacture of bimetal transition pieces from austenitic steel-α-titanium alloy. *Svarochn. Proizvodstvo*, **4**, 34–36 [in Russian].
10. Rodin, M.E., Semenov, A.N., Plyshevsky, M.I. et al. (2008) Investigation of mechanical properties of corrosion-resistant steel welded joints with titanium alloys. *Ibid*., **6**, 9–11 [in Russian].
11. Lyushinsky, A.V., Mazanko, V.F., Belyakova, M.N., Vorona, S.P. (1999) Mass transfer in pressure welding using ultrafine nickel powders. *Ibid*., **6**, 10–14 [in Russian].
12. Lyushinsky, A.V. (2013) *Modern welding technologies. Engineering-physical principles*. Moscow, ID Intellekt [in Russian].
13. Lyushinsky, A.V. (2001) Criteria of selection of interlayers in diffusion welding of dissimilar materials. *Svarochn. Proizvodstvo*, **5**, 40–43 [in Russian].

Received 31.01.2019

DOI: http://dx.doi.org/10.15407/tpwj2019.04.05

CALCULATION OF CHARACTERISTICS OF ALTERNATING TRANSVERSE MAGNETIC FIELD, HAVING EFFECT ON DROP TRANSFER IN ARC WELDING AND SURFACING

A.D. RAZMYSHLYAEV[1] and **M.V. AHIEIEVA**[2]
[1]SHEI «Priazov State Technical University»
7 Universitetskaya Str., 87500, Mariupol, Ukraine. E-mail: razmyshljaev@gmail.com
[2]Donbass State Mechanical Academy
72 Akademicheskaya Str., 84413, Kramatorsk, Ukraine. E-mail: maryna_ah@ukr.net

It is shown that in submerged-arc surfacing with the effect of constant transverse magnetic field the coefficient of melting of electrode wires of 3–5 mm diameter is increased by 25–30 %. It is experimentally found that at the effect of an alternating field at unchanged level of a transverse component of induction, the effect of increase in the coefficient of melting depends on frequency of this field. With increase of the field frequency up to 10–20 Hz, the increment of the coefficient of melting decreases to zero values. A procedure was developed for determination of the minimum level of transverse component of field induction in the electrode drop zone, at which the drop is detached from a melting electrode end. It is shown that the effect of decreasing the coefficient of melting at increase in the field frequency is predetermined by the reduction in duration of pulses. The paper gives the calculated data, allowing determination of optimum values of induction and frequency of the alternating field, at which the coefficient of wire melting at submerged-arc surfacing (welding) is increased. 8 Ref., 4 Figures.

Keywords: *arc surfacing (welding), transverse magnetic field, induction, electrode melting coefficient, frequency, calculation procedure*

The use of transverse magnetic field (TMF) in arc surfacing and welding allows controlling the geometry of beads and welds [1], refining the structure of weld metal (bead) [2–4] and increasing the strength of welded joints [5].

An important problem is increasing the efficiency of the electrode wire melting process during submerged arc welding and surfacing. Currently, the main attention of researchers is devoted to the development of TMF input devices (ID). However, there are no investigations devoted to clarifying the causes for increase in the melting coefficient of electrode wires during arc surfacing and welding under the TMF effect.

In the works [5, 6], the values of coefficient of the electrode wire melting α_m during submerged-arc surfacing with the effect of the controlling TMF were experimentally determined. It is shown that its use allows increasing the coefficient of wires melting. The maximum increase in the coefficient α_m (up to 30 %) is observed at the use of constant TMF, with the growth in frequency of this field, the effect of increase in α_m decreases to zero values at frequency of 20–50 Hz. In these works, a calculation procedure is presented, which makes it possible to explain the physical principle (causes) of increase in the coefficient α_m from the effect of constant TMF during arc surfacing. However, the calculation procedure given in the works [5, 6] can be used only in the case when a constant TMF is applied during surfacing, when at the electrode end a bevel is formed. It is impossible to apply this procedure to the alternating TMF, which hinders their rational use in arc surfacing and welding.

The aim of the work is to develop a calculation procedure that allows determining the minimum level of a transverse component of induction of TMF of different frequencies, which removes a drop from the electrode wire end and, due to that, increasing the coefficient of melting the electrode wires during submerged arc surfacing and welding.

As in the works [5, 6], in the present investigation the coefficient α_m of melting electrode wires Sv-08A of the diameters of 3–5 mm in arc surfacing under the flux AN-348 at a direct current of reverse polarity was experimentally determined.

The values of α_m of wires were determined by the well-known procedure (weighing method). In this case, surfacing was performed with the effect of both constant and alternating TMF at the frequency of 2; 5; 12; 24; 33 and 50 Hz. The same TMF ID, as in the works [5, 6], as well as the device supplying the coils of TMF ID, were used. The deposits were produced also without TMF effect. In order that a workpiece (plates being deposited) did not distort the structure of the magnetic field in the zone of an electrode drop

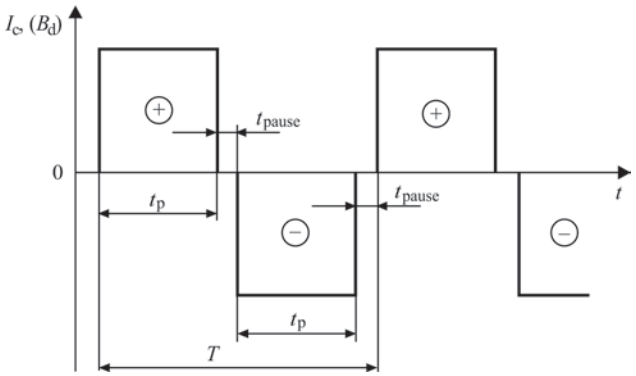

Figure 1. Diagram of current pulses I_c, supplying the coils of TMF ID

and weld pool, the plates of steel 12Kh18N10T (nonmagnetic) of 12–20 mm thickness were used. A diagram of rectangular pulses (current I_c in the coils of TMF ID and induction B_d) is shown in Figure 1. Here, the induction B_d was measured using a universal teslameter of 43205 type with Hall sensor, which had a measuring base of 0.9×0.9 mm near the base metal surface (in the future weld pool zone) under the electrode wire at a distance from its end to the plate Δ = = 5 mm. The induction B_d was measured during direct current passing in the coils of TMF ID; therefore, the maximum values of B_d in pulses, shown in Figure 1, correspond to the values which were during passing of direct current in the coils.

In all the experiments, the same values of induction B_d = 30 mT were maintained. There was a possibility of changing the duration of pulses (I_c, B_d) – t_p, and the pause t_{pause}. The duration of pauses t = 0.01 s was set (Figure 1). The duration of the period was T = = 2 (t_p + t_{pause}); frequency f = 1/T.

It was experimentally found that under the effect of constant TMF and induction B_d = 30 mT, the maximum increment in the coefficient α_m (Figure 2) is observed, which corresponds to the data established in the works [5, 6]. The values of α_m of wires during surfacing without TMF effect were also determined. The data showed (not given here) that the values of α_m

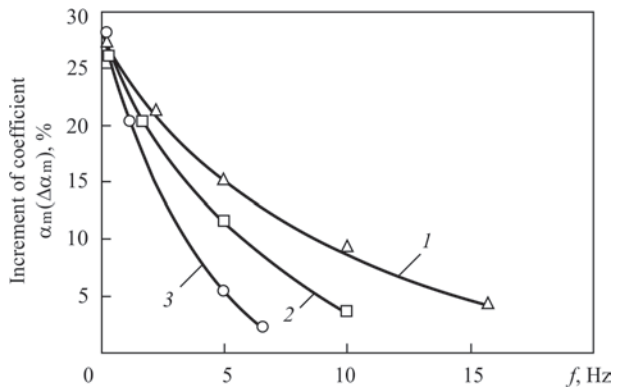

Figure 2. Effect of frequency f of TMF on increment of the coefficient α_m ($\Delta\alpha_m$) (I_s = 480–520 A; U_a = 30–32 V, B_d = 30 mT): *1*, *2*, *3* — diameters of electrodes, respectively, 3, 4, 5 mm

of wires with the diameter of 3–5 mm in surfacing at I_s = 300–500 A are in the range of 12.5–14.5 g/(A·h), which corresponds to the well-known regularities[8].

With increase in frequency of TMF, the effect of increasing α_m of the electrode wires decreases, but its decrease is more sharp than it was previously established in the works [5, 6] (Figure 2). The decrease in the effect of increasing α_m of wires is associated with features of a forced removal of drop from the melting end at the effect of different frequency of TMF.

Below a calculated procedure is presented, that allows explaining the effects of TMF on the coefficient α_m of melting the electrode wires in arc surfacing (welding).

In the present investigation, as was noted, the values of pauses duration t_{pause} = 0.01 s was used. This is connected with the fact that during the pause of the effect of TMF (short pause, t_{pause} = 0.01 s) a significant layer of liquid metal was not accumulated at the end of the electrode. The analysis shows that in surfacing (welding) using the wires of the diameters of 3; 4 and 5 mm and at the current I_s = 500 A; the speed of electrodes feeding is approximately $v_{e.f}$ = 2·10^{-2} m/s (2 cm/s). Then, if t_{pause} = 0.01 s, then at the end of the electrode, a layer of liquid metal with a thickness of $h = v_{e.f} t_{pause}$ = 2·10^{-2}·10^{-2} = 2·10^{-4} = 0.2 mm is formed, which can be neglected.

Then, simply, it can be accepted that t_{pause} = 0 and the frequency of TMF

$$f = \frac{1}{T} = \frac{1}{2\left(t_p + t_{pause}\right)}, \quad (1)$$

$$f = \frac{1}{2t_p}, \quad (2)$$

and the pulse duration

$$t_p = \frac{1}{2f}, \quad (3)$$

where f is the frequency of TMF, Hz.

In the works [5, 6], it was found that the bevel of the electrode end in arc melting of wire is not formed if the frequency of TMF is higher than 1–2 Hz. This regularity is taken in the present investigation.

Let us assume that at the end of a melting electrode before the effect of TMF pulses (B_d), a drop in the form of hemisphere was present with a sphere radius $r = d/2$ (d is the diameter of the electrode wire, m).

In this case, the drop volume

$$V_{drop} = \frac{1}{2}\frac{4}{3}\pi r^3; \quad V_{drop} = \frac{1}{12}\pi d^3 \text{ m}^3. \quad (4)$$

The drop mass

$$m = \rho V_{drop}, \text{ kg}, \quad (5)$$

where ρ is the density of drop liquid metal, kg/m^3, ρ = = 7·10^3 kg/m^3.

The electromagnetic force acts (horizontally) on the drop (in the direction of *X* axis):

$$F'_{em} = F_{em} V_{drop}, \text{ N}, \quad (6)$$

where F_{em} is the density of electromagnetic force in the drop, N/m^3.

At the given current of surfacing I_s and at the action of induction B_d:

$$F'_{em} = \frac{4I_s}{\pi d^2} B_d \rho V_{drop}, \text{ N}. \quad (7)$$

Under the action of force F'_{em} a drop of volume V_{drop}, will receive an acceleration

$$a = \frac{F'_{em}}{m}, \text{ m}/\text{s}^2. \quad (8)$$

Then

$$F'_{em} V_{drop} = \rho V_{drop} a; \quad F'_{em} = \rho a. \quad (9)$$

Taking into account (7) and (9), we shall receive:

$$a = \frac{F'_{em}}{\rho} = \frac{4I_s B_d}{\pi d^2}, \text{ m}/\text{s}^2. \quad (10)$$

The drop under the action of the force F'_{em} is removed (horizontally along the axis *X*) at a speed

$$V = \sqrt{2La}, \text{ m}/\text{s}, \quad (11)$$

where *L* is the length of the drop «acceleration» at the electrode end, m.

Obviously, that *L* = *d*, then

$$V = \sqrt{2da}, \text{ m}/\text{s}. \quad (12)$$

The time of a drop removal from the electrode end (displacement along path *L* = *d*):

$$t = \sqrt{\frac{2d}{a}}, \text{ s}. \quad (13)$$

The minimum level of induction B_d, that removes a drop at a given frequency is:

$$B_d = \frac{2\rho\pi d^3 f^2}{I_s}, \text{ T}. \quad (14)$$

By the formula (14), the value of the induction B_d (as the minimum level) was calculated, which removes a drop from the electrode end as-applied to the arc surfacing with wire Sv-08A of diameters 3–5 mm, current I_s = 300–1000 A and different frequency *f* of TMF. The data shows (Figure 3) that with the growth in current I_s (as it should be expected from the formula (14)) and the given frequency of TMF, the level of induction B_d, at which a drop is removed from the electrode end, decreases. As the frequency *f* of TMF increases from 5 to 10 Hz, the level of induction B_d increases significantly. This is clear, because with the growth in frequency *f* of TMF, the duration of a pulse action (t_p) of TMF decreases.

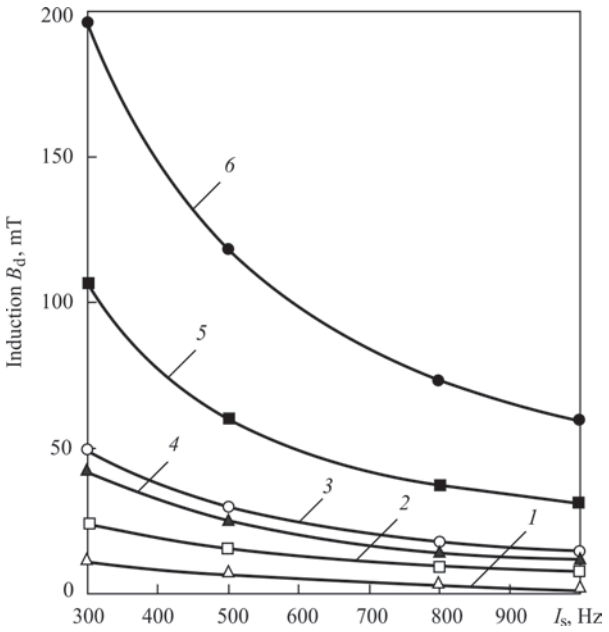

Figure 3. Dependence of induction B_d on surfacing current I_s: *1*, *4* — *d* = 3 mm; *2*, *5* — *d* = 4 mm; *3*, *6* — *d* = 5 mm; *1*, *2*, *3* — *f* = = 5 Hz; *4*, *5*, *6* — *f* = 10 Hz

At a preset current (I_s = 500 A in Figure 4), an increase in the frequency *f* of TMF leads to a sharp increase (according to the quadratic dependence in compliance with the formula (14)) in induction B_d of TMF. This is also caused by a sharp decrease in duration of pulses (t_p) of TMF at the increase in the frequency *f* of TMF. From Figure 4, it follows that at the level of induction B_d = 30 mT (and current I_s = = 500 A), at which deposits were produced (Figure 2), a decrease in the growth of α_m is associated with an insufficient level of induction B_d.

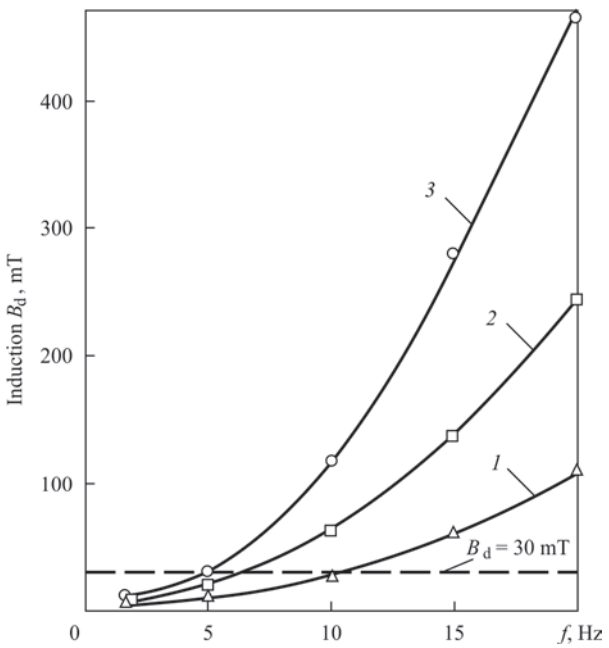

Figure 4. Dependence of induction B_d on frequency *f* (I_s = 500 A): *1*, *2*, *3* — diameters of wires, respectively, 3, 4, 5 mm

Thus, the effect of increase in the coefficient α_m under the conditions of action of the alternating TMF during arc surfacing and welding consists in a sufficient level of the induction B_d in a pulse of TMF and in a pulse duration t_p (and, accordingly, frequency value) of TMF.

The developed calculation procedure for determination of the minimum level of induction B_d in TMF at a preset frequency of TMF makes it possible not only to explain the observed effects of alternating TMF on the efficiency of melting the electrode wires during submerged-arc surfacing, but also to recommend optimal parameters of such TMF for arc surfacing (and welding).

It should be noted that the observed effects of increasing α_m during submerged-arc surfacing occur when other wires are used (both ferromagnetic and non-ferromagnetic, for example, 06Kh18N10T). It is obviously, that if the duration of pauses (t_{pause}) of rectangular pulses at a preset frequency (or close to the frequency f of TMF) is increased, then the effect of TMF on α_m of the wires in arc surfacing (at a given frequency and a level of the induction B_d) will decrease. As the optimal value, t_p = 0.01–0.02 s should be taken.

It should be noted that in welding and surfacing, only alternating TMF improves the formation of welds and deposited beads. Alternating TMF induces flows of liquid metal in the weld pool from its head part to the tail part and back again. This leads to the refinement of structural components of the weld metal (deposited bead), thus improving the mechanical properties of welds and deposited metal [3, 5]. Here, the use of alternating TMF with a frequency of up to 20 Hz [3, 5, 7] is effective.

In the present work, as in the works [5, 6], TMF ID was used, on the rods of which the windings (coils) of insulated copper wire with a number of turns W = = 100–150 were placed. To prevent the windings from overheating, the current in them should not exceed 20 A. In this case, in the zone of an electrode drop and in the head part of the pool, a transverse component of the TMF induction (B_d) of about 30 mT is provided, sufficient to control the transfer of electrode drops and to induce flows in the liquid metal of the pool (at f = 10–20 Hz). The increase in the number of turns in the windings or the diameter of their wire increase the bulkiness of design of TMF ID (striving to reach the level of B_d = 60 mT and higher, see Figure 4). Therefore, it should be recommended to apply TMF with the frequency of not higher than 15–20 Hz (better — 5–10 Hz). In this case, the increase in α_m reaches the values of up to 15 g/(A·h), which improves the efficiency of arc surfacing and welding processes. It should be noted that for the convenience of performing these processes, it is desirable to use a transverse arrangement of rods of TMF ID with respect to the weld (bead) axis.

Conclusions

1. In submerged-arc surfacing at the increase in frequency of alternating transverse magnetic field, the effect of growing the coefficient of electrodes melting decreases to zero values at the frequencies of the order of 10–20 Hz of TMF.

2. A calculation procedure was developed, which allows determining the minimum value of a transverse component of the TMF induction, which removes a drop from the melting end of the electrode wire at a preset frequency of this field. The calculated values of the minimum level of induction of the alternating TMF are given, which made it possible to explain the effects of such TMF on the coefficient of melting the electrode wires during arc surfacing (welding)

3. In submerged-arc surfacing and welding, in order not only to provide the removal of electrode drops from the end of the electrodes and to increase their melting efficiency, but also for efficient mixing of liquid metal in the pool, it is rational to use the alternating TMF of up to 10 Hz frequency.

1. Razmyshlyaev, A.D. Ahieieva, M.V. (2018) Effect of transverse magnetic field on weld geometry in repair of products. *Visnyk Pryazov. DTU*, **44**, 77–79 [in Russian].
2. Razmyshlyaev, A.D., Ahieieva, M.V. (2018) *TMF influence on weld structure at the welding of 12Kh18NT*. Mat. Sci. Forum, 927, 1–5, https://doi.org/10.4028/www.scientific.net/MSF.927.1
3. Razmyshlyaev, A.D., Ageeva, M.V. (2018) On mechanism of weld metal structure refinement in arc welding under action of magnetic fields (Review). *The Paton Welding J.*, **3**, 25–28.
4. Morozov, V.P. (2006) Analysis of conditions of refined structure formation in crystallization of weld pool metal under superposition of external periodic perturbations. *Izv. Vuzov. Mashinostroenie*, **8**, 41–54 [in Russian].
5. Razmyshlyaev, A.D., Vydmysh, P.A., Ahieieva, M.V. (2018) *Automatic submerged-arc welding under action of external magnetic field*. Mariupol, PGTU [in Russian].
6. Razmyshlyaev, A.D., Serenko, A.N., Vydmysh, P.A., Ahieieva, M.V. (2015) Calculation of transverse magnetic field providing drop detachment from electrode tip in arc surfacing. *Visnyk Pryazov. DTU*, **30**, 7–14 [in Russian].
7. Razmyshlyaev, A.D., Ahieieva, M.V. (2018) To calculation of numerical values of induction of transverse control magnetic field in head part of welding pool. *Nauka ta Vyrobnytstvo: Transact.*, **19**, 51–59 [in Russian].
8. Akulov, A.I., Belchuk, G.A., Demyantsevich, V.P. (1977) *Technology and equipment of fusion welding: Manual for students of higher education institutes*. Moscow, Mashinostroenie [in Russian].

Received 06.03.2019

DOI: http://dx.doi.org/10.15407/tpwj2019.04.06

REPAIR OF SCREWS OF EXTRUDERS AND AUTOMATIC MOLDING MACHINES BY PTA SURFACING

A.I. SOM
Plasma-Master Ltd Company
3 Krzhyzhanovskogo Str., 03142, Kyiv, Ukraine. E-mail:info@plasma-master.com

The peculiarities of formation of a bead on narrow tip of screw flight in PTA surfacing were investigated. It is shown how a shape of deposited bead depends on its section and main technological parameters of surfacing, i.e. arc current, surfacing speed and PTA torch zenith displacement. The nomograms for selection of surfacing mode parameters were proposed. Equipment and consumables used for surfacing are also described. Repair of screws of extruders and automatic molding machines using PTA surfacing allows repairing these parts as well as 3–5 times increasing their service life in comparison with new nitrated screws. 11 Ref., 13 Figures.

Keywords: *PTA surfacing, screws of extruders and automatic molding machines, narrow tip, bead formation, surfacing parameters, equipment and consumables*

In process of operation the screws of extruders and automatic molding machines are subjected to intensive wear-out, in particular, during processing of composite plastics with fillers having abrasive effects. Wear of these parts takes place mainly on the flight tips, which resulted in increase of working gap between the screw and cylinder and, as a consequence, drop of productivity of screw extruder in whole. Regardless nitration, which is used to raise wear resistance, their service life in a series of cases does not exceed 6–8 months. These parts are complex on design (Figure 1) and expensive, therefore, repair and increase of their service life is a very relevant problem.

The most efficient method for repairing the screws is surfacing of a thin layer (1–2 mm) of wear- and corrosion resistant alloy on flight tip. The best for this is a method of PTA surfacing (PTAS), which due to its technological peculiarities allows providing excellent formation of deposited bead at minimum melting of flight tip [1–5].

Surfacing on flight tip of screw is sufficiently difficult technological problem due to design peculiarities of these parts. First of all, this is a large relationship of length to diameter reaching in modern machines 30, and the varying sizes of flights on part length, namely width and height. The surfacing is also complicated by wide range of screws, in which diameter can be changed from 20 to 300 mm, length from 600 to 6000 mm and width and height of flights from 3 to 30 mm.

Earlier E.O. Paton Electric Welding Institute and then Plasma-Master Ltd with participation of the author of this paper have carried the large complex work on optimizing the PTAS process of screws with development of special surfacing alloys and equipment. Surfacing in repair of screws shall be performed directly on flight tip, i.e. on the surface with limited width and large curvature. Under these conditions it is very difficult to provide set size and shape of bead, in particular, in surfacing of parts of small diameter (20–40 mm), having flight width only 3–4 mm. In order to solve this problem it was necessary to investigate the peculiarities of bead formation on narrow substrate and set the relationship between its shape and main technological parameters of the process of plasma surfacing.

Formation of bead on flight tip of screw. Cross-section profile of deposited bead is formed under effect of many factors, namely surface tension of weld pool met-

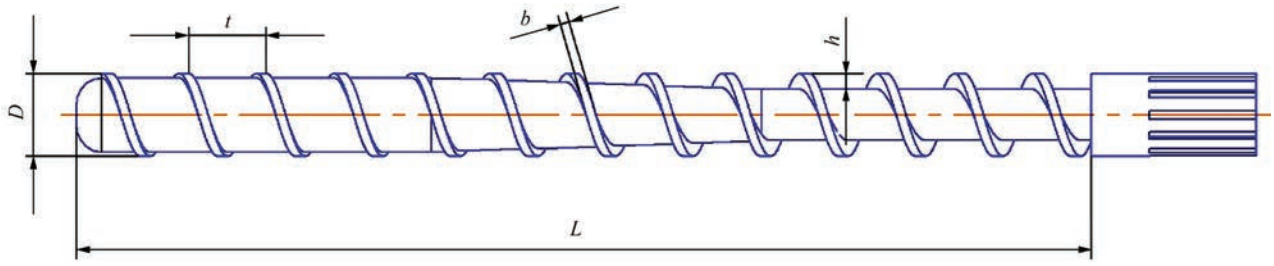

Figure 1. Typical screw of extruder for processing of polymers

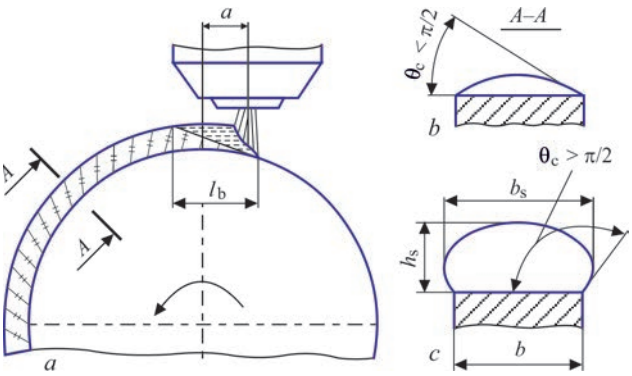

Figure 2. Scheme of surfacing on tip of screw flight (*a*) and shape of deposited beads at small (*b*) and close to optimum (*c*) cross-section area

al, gravity force, arc pressure, etc. [6–8]. The main peculiarity of formation lies in the fact that bead width in its bottom always equals to a flight width (Figure 2).

In this case the most important parameter, which determines a bead shape, is its fullness, i.e. cross-section area S_s. Rise of S_s provokes increase of height h_s as well as change of coefficient of bead shape K ($K = b_s/h_s$) and angle of bead contact with substrate θ_c (Figure 3).

Bead shape becomes more favorable from point of view of machining allowances ($b_s > b_b$), but there is rise of danger of dripping of weld pool metal in the process of surfacing. Therefore, in surfacing with free formation of bead section its height, respectively, can be increased only to some level depending on width of flight screw bead and metal capillary constant of the weld pool metal.

Figure 4 shows the optimum for deposited metal of 220Kh18FM2N3 [9, 10] type values of $S_{s.o}$ and $h_{s.o}$ at which favorable formation of beads is provided ($\theta_c > 90°$; $b_s > b$) and there is no dripping of weld pool liquid metal in side directions. However, bead cross-section at this flight width ambiguously determines its shape. The latter in many respects depends on technological parameters of the process, i.e. arc current I_a, surfacing rate V_s, arc zenith displacement a (Figure 1, *a*), etc.

Base metal penetration in PTA surfacing on the optimum modes is insignificant [11], therefore cross-section area of beads is proportional to value of relationship of powder feed G_f to surfacing rate V_s. Keeping this relationship constant it is possible to obtain deposited beads with set S_s at different deposition rate of surfacing process. However, increase of filler

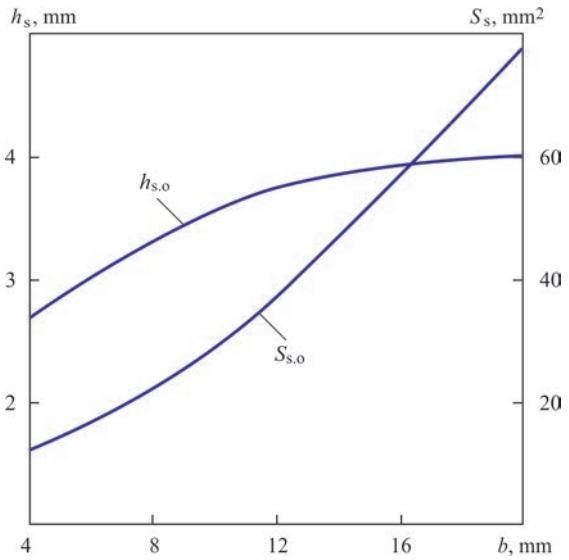

Figure 4. Optimum cross-section areas $S_{s.o}$ and height $h_{s.o}$ of deposited bead for different width of flight tip *b*

powder feeding requires increase of arc current, that, in turn, results in rise of weld pool length (Figure 5).

As can be seen from Figure 5, length of weld pool is particularly large at small width of flight (up to 8 mm), when surfacing is performed without transverse oscillations of PTA torch on relatively high currents. If length of the weld pool reaches critical value L_{cr} for this diameter of part D, the process of surfacing is disturbed because of dripping of liquid metal (Figure 6), which can not be prevented due to arc zenith displacement. Based on our data $L_{cr} = (0.22–0.26)/D$.

Surfacing of flights of more than 8 mm width is performed with transverse oscillations of PTA torch thanks to which the weld pool has smaller length at similar currents (see Figure 5). Besides, in these cases the deposited parts, as a rule, have larger diameter, therefore in practice the critical length of the pool is usually not achieved.

In turn, the weld pool length considerably depends on flight height that is related with change of conditions of heat sink into the part. Increase of flight height provokes also rise of pool length, however, at that lower current is necessary (Figure 7).

The higher the flight, the more obvious pool elongation is. In real parts the flight height is usually changed from 2 to 3 mm (dosing zone) up to 15–20 mm (filling zone). Under these conditions the length of weld pool at similar surfacing rate in one

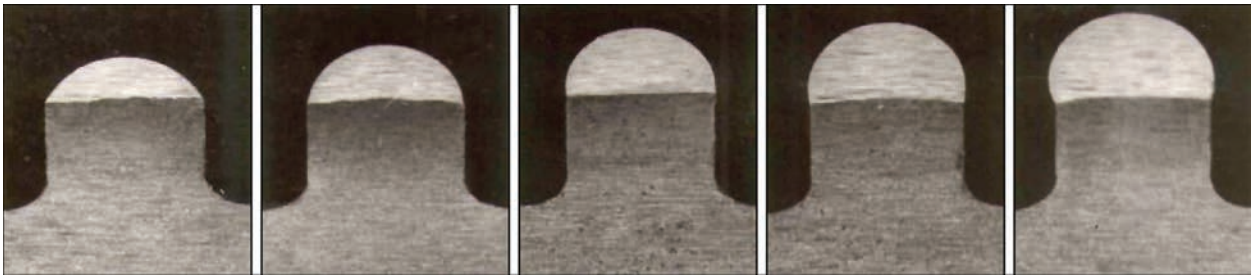

Figure 3. Macrosections of deposited beads with different area of cross-section

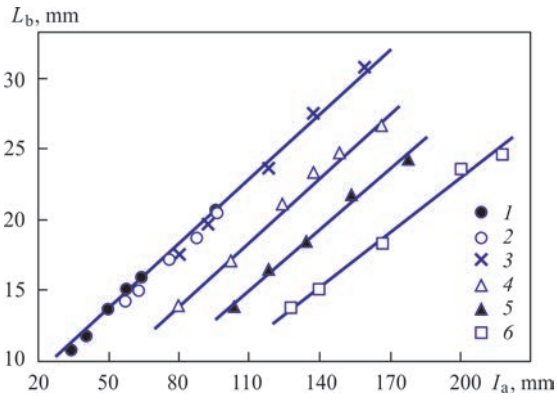

Figure 5. Dependence of weld pool length L_p on arc current I_a in tip width b [6]: *1* — b = 4; *2* — 5; *3* — 7; *4* — 10; *5* — 15; *6* — 20 mm

place of the screw can be less critical, and in the other, vice versa, more critical.

In addition to length of a weld pool selection of the optimum parameters of surfacing mode requires also considering the shape of bead cross-section, which determines machining allowances. It to larger extent depends on surfacing rate and PTA torch zenith displacement. Effect of these parameters on bead shape with similar area of cross-section is shown on macrosections (Figure 8).

As can be seen (Figure 8, *a*) rise of V_s at constant displacement of PTA torch from zenith *a* deteriorates the bead shapes. They became more convex and provoke decrease of side overhanging of the deposited metal. It takes place due to elongation of tail part of the weld pool since rise of V_s obligatory requires increase of welding current.

Increase of PTA torch zenith displacement to the side opposite to part rotation vice versa improves the bead shape (Figure 8, *b*). They became wider and flatter since they are formed under conditions of higher arc pressure. However, the displacement can be increased only to some extent, which does not violate the equilibrium between hydrostatic pressure of liquid metal of weld pool and arc pressure. Based on our data the displacement should not exceed $2/3L_b$. In practice, it is approximately (0.10–0.12)D. In the other case it will be difficult to hold the pool on the flight surface and liquid metal start dripping. This parameter is particularly important in surfacing of the small diameter parts of 40–60 mm. Zenith displacement can be increased to 0.2D at rise of part diameter and width of flight, when surfacing is carried out with PTA torch oscillations.

Thus, effect on the surfacing process of arc current, surfacing rate and PTA torch zenith displacement, the three parameters which are tightly connected with each other, becomes apparent through change of size and shape of the weld pool.

Carried investigations show that there is comparatively narrow area of surfacing modes for each dimension type of the part, which provides favorable

Figure 6. Appearance of deposited beads at pool length less than critical (*a*) and more (*b*); d = 90 mm; b = 7 mm

bead shape and absence of liquid metal dripping. The results of investigations of effect of surfacing technological parameters on bead formation were processed using a mathematical statistics method. The calculation considers not only the modes of surfacing, which provided the optimum section of deposited bead, its good formation and minimum penetration of the base metal. Number of points for observation made 78. Obtained data were used for plotting nomograms for selection of surfacing modes convenient for practical application (Figure 9).

For example, they show a sequence of selection of a mode for surfacing of 90 mm diameter screw with flight tip width 8 mm. The surfacing parameters, namely powder feed and PTA torch zenith displacement are constant along the whole screw length, and arc current at transfer from filling zone to dosing zone shall increase from I_1 to I_2 in accordance with decrease of flight height h_1 to h_2.

As it was already mentioned, at flight width more than 8 mm the surfacing is carried out with PTA torch oscillations. In this case amplitude A and oscillation frequency f are determined on formulae:

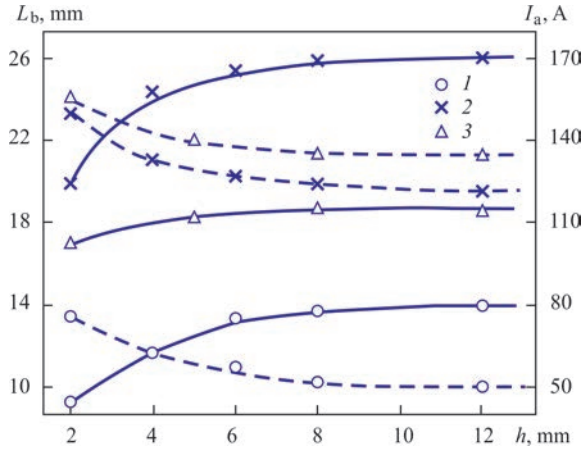

Figure 7. Dependence of weld pool length L_p (solid) and arc current I_a (dashed) on flight height h at tip width b: *1* — b = 4; *2* — 7; *3* — 15 mm

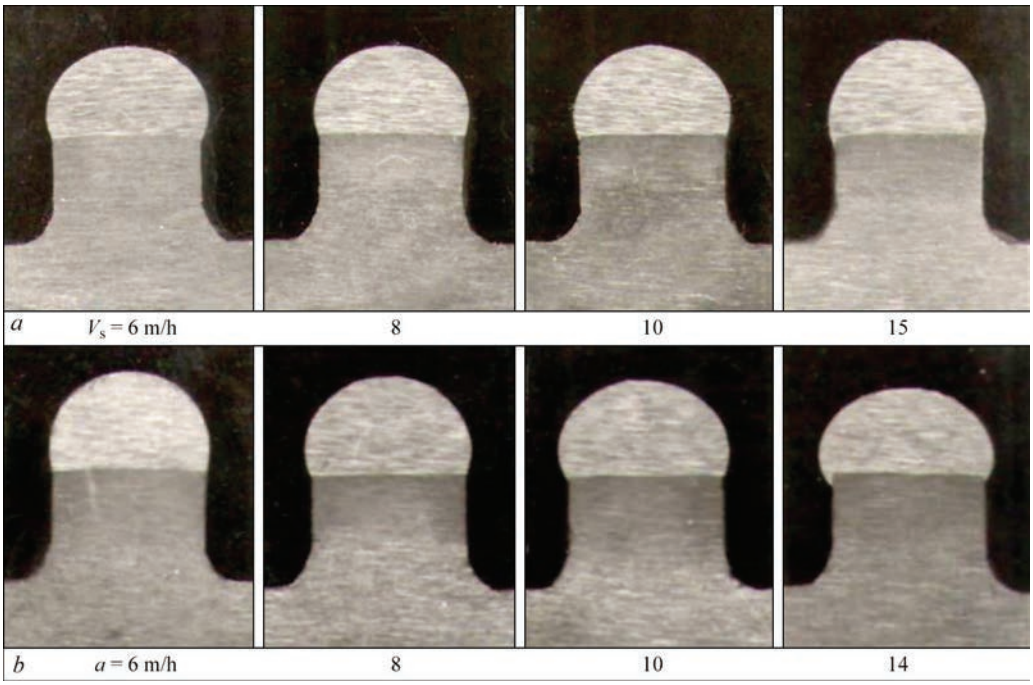

Figure 8. Macrosections of beads of similar section deposited on tips of flights of 7 mm width with different rates (*a*) (zenith displacement 11 mm) and different displacement from zenith (*b*) (surfacing rate 8 m/h)

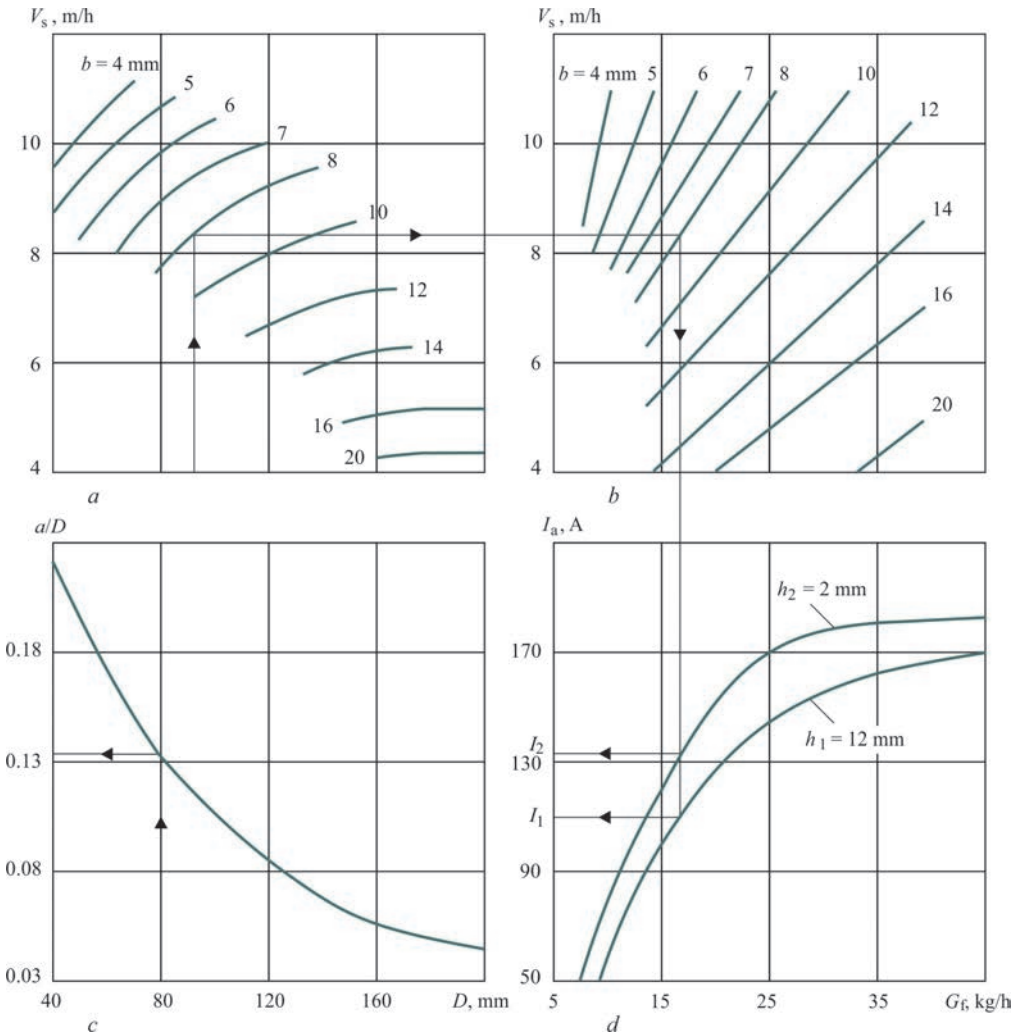

Figure 9. Nomograms for selection of parameters of screw surfacing mode: *a* — surfacing rate V_s; *b* — powder feed G_f; *c* — PTA torch displacement from zenith *a*; *d* — arc current I_a

$$A = \frac{b - d_{pl}}{2}, \text{ mm}; \quad f = \frac{V_s}{t_s}, \quad \text{min}^{-1},$$

where b is the width of flight tip; d_{pl} is the diameter of plasma forming nozzle; V_s is the surfacing rate; t_s is the surfacing step (1.5–2.0 mm).

The proposed procedure allows orienting in the selection of the optimum parameters of surfacing mode, which in practice shall be specified depending on thermophysical properties of base and filler materials, fraction of powder and PTA torch design.

Equipment for surfacing. Plasma-Master Ltd. Company has developed two types of equipment for PTA surfacing of screws of extruders and automatic molding machines. These are installations developed based on turning lathes having own bed with rotator and rear center.

In the first case the lathe is used as a ready-made bed, on support of which specially developed surfacing apparatus RM-300 is installed. It contains PTA torch, oscillation mechanism with corrector, power feeder, lifting mechanism and control panel. The dimensions of lathe are selected depending on the maximum length of deposited parts. Kinematics of the lathe after small transformations allows rotating the part with necessary rate and moving the apparatus with PTA torch with set surfacing step. The process of surfacing is regulated from one panel located on the apparatus.

The control system is made on the basis of PLC, which allows accurately adjust to a pitch of screw flights and follow the process parameters. The installation also includes a control cabinet, inverter welding power source and autonomous cooling unit of the PTA torch. Such type of installation is reasonable for development if the Customer has available turning lathe of necessary length. Regardless, some inconveniencies in work, such an approach allows significantly reducing total cost of the installation. Figure 10 shows an example of such installation.

In other cases it is more reasonable to use special installation RM-307 (Figure 11). It initially contains all necessary mechanisms driven from general panel. Step motors are used as drivers. The guides, on which the surfacing apparatus is moved, are located on a beam in the top part of the installation that allows preventing falling on them of filler powder and, thus, their preliminary wear-out.

The installation uses a rotator with tilt axis, which permits surfacing of cylinder as well as conical edge surfaces. In becomes more versatile in such a variant. The installation can surface the cylinder parts of 20–300 mm diameter and 4500 mm length in automatic and semi-automatic modes. Number of steer axes can be from 3 to 5.

Consumables. Following the conditions of operation and design peculiarities of screws of extruders and automatic molding machines, the alloys designed

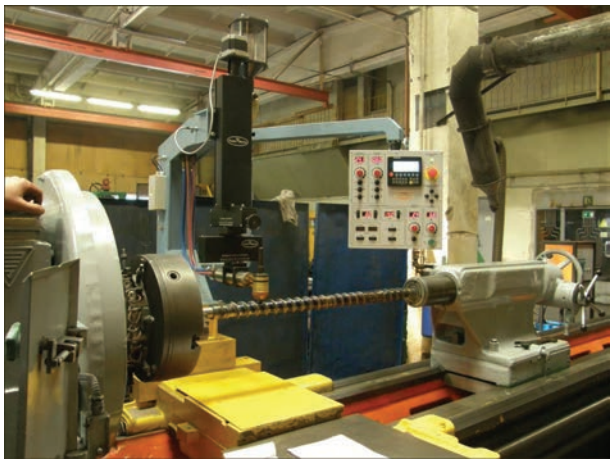

Figure 10. Installation for PTA surfacing based on turning lathe and apparatus RM-300

for their surfacing shall satisfy a series of requirements. In addition to high wear-resistance, they shall have sufficient corrosion resistance at processing of aggressive polymers, good compatibility at friction with cylinder metal and high technological properties in surfacing. Nickel and cobalt based alloys are the most often used in the world practice for these purposes. In order to eliminate cracks in the deposited layer the parts are preheated till 400–500 °C temperature and sometimes concurrent heating is used.

The experience shows that preheating of such parts not only complicates the surfacing process, but significantly raises its price. Wear- and crack-resistant alloy based on iron of Fe–Cr–V–Mo–C system [9, 10], was developed especially for PTAS of screws with the participation of author. Today, it is produced in form of powder of PR-Kh18FNM grade (PMalloy21). This alloy refers to high-vanadium cast iron class. The peculiarity of structure of this alloy is very fine grain (10–15 μm) and fan-shaped form of eutectics, located as separate colonies like being implemented in austenite-martensite matrix (Figure 12).

Such eutectic structure provides alloy with combination of high strength and ductility σ = 1000 MPa and $\alpha_s = 25 \cdot 10^2$ MPa. Metal hardness after surfacing makes *HRC* 43–45. After tempering at 650 °C temperature for 2 h its hardness due to secondary hard-

Figure 11. Installation RM-70 for PTA surfacing of screws of extruders and automatic molding machines

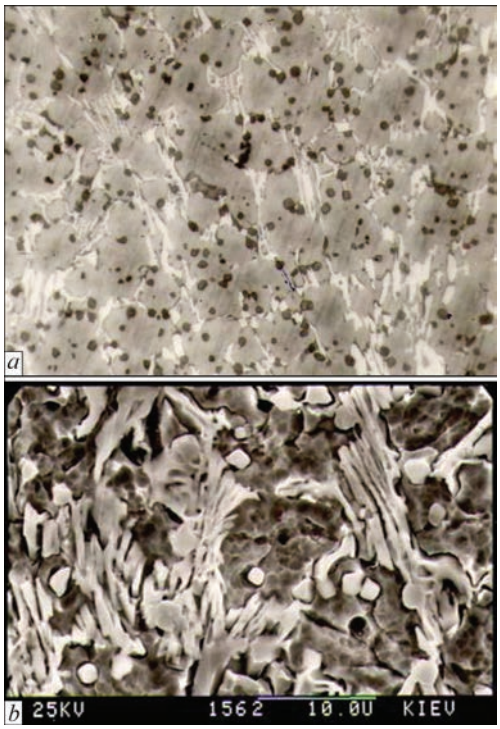

Figure 12. Microstructure of metal, deposited with powder PR-Kh18FNM (PMalloy21): *a* — optical microscope (×500); *b* — electron microscope (×3000)

ening rises to *HRC* 52–53. The main wear-resistant phase of the alloy is vanadium carbides VC.

Powder of PR-Kh18FNM grade (PMalloy21) is widely used in industry for surfacing of screws in Ukraine, Russia, Poland and other countries. A huge experience on surfacing and operation of deposited parts in processing of pure as well as filled polymers has been accumulated for more than 20 years period. The powder provides excellent formation of deposited metal (Figure 13) and absence of cracks even in small massive parts at correct choice of surfacing modes. This important technological advantage of given alloy allows rejecting from preheating of billet and, thus, significantly simplify surfacing process.

It should also be noted that surfacing allows not only repairing the expensive part, but considerably rising its wear resistance. In comparison with new nitrated screws the repaired parts demonstrate 3–5 times higher resistance depending on type of processed material. It is also 1.2–1.5 time higher when comparing with the screws deposited with PG-SR3 and Stellite 6 alloys.

Conclusions

1. Shape of bead at plasma surfacing on narrow tip of screw flight depends on fullness (cross-section area), deposition rate and PTA torch zenith displacement. To provide the best bead formation it is necessary that zenith displacement equals to approximately 2/3 of weld pool length, and length of the pool itself shall not exceed 0.22–0.26 of part diameter.

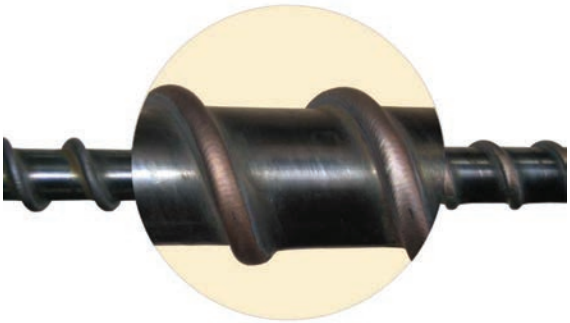

Figure 13. Fragment of deposited screw of 63 mm diameter

2. The proposed procedure for selection of screw surfacing modes allows orienting on the selection of the main process parameters, namely arc current, deposition rate, powder feed and PTA torch zenith displacement depending on part geometry, i.e. diameter, width and height of flights.

3. Developed equipment, technology and surfacing powder PR-Kh18FNM (PMalloy21) allow efficient repair of worn-out screws as well as significant rise of their wear resistance in comparison with new nitrated parts.

1. Luelsdorf, P. (1975) Verschleissprobleme mit Zylinder und Schnecke beim Extrudieren. *Reilloy-Bericht*, **4**, 1–8 [in German].
2. (1977) Plasma arc weld surfacing – new route to hardfacing screws. *Plastics Technology*, 23(**10**), 17–19.
3. Frumin, I.I., Som, A.I., Gladky, P.V. (1981) Plasma surfacing of screw extruders of polymer machines. In: *Theoretical and technological principles of surfacing. Surfacing in machine-building and repair: Transact*. Kiev, PWI, 13–21 [in Russian].
4. Som, A.I., Gladky, P.V., Pereplyotchikov, E.F. (1985) Increase of service life of extruders by plasma surfacing. In: *Surfacing. Experience and efficiency of application*. Kiev, PWI. 89–93 [in Russian].
5. Gorka, J., Czuprynski, A., Kik, T., Melcer, M. (2011) Przemyslowe aplikacje napawania plazmowego proszko-wego. *Przeglad Spawalnictwa*, **9**, 87–94 [in Polish].
6. Som, A.I., Gladky, P.W. (1984) Peculiarities of plasma surfacing on narrow substrate. *In: New processes of surfacing, properties of deposited metal and transition zone*. Kiev, PWI, 20–24 [in Russian].
7. Emelyanov, I.A. (1972) Influence of forces of surface tension and external pressure on shape of deposited bead surface. In: *Transact. of LIVT Tekhnologiya Sudostroeniya i Remonta*, **135**, 135–145 [in Russian].
8. Yakobashvili, S.B. (1974) Influence of forces of surface tension and external pressure on shape of deposited bead surface. *Welding processes in metallurgy*. Tbilisi, Metsniereba, **1**, 89–99 [in Russian].
9. Som, A.I., Gladky, P.V., Pereplyotchikov, E.F. (1983) New wear-resistant alloy for plasma surfacing. In: *Theoretical and technological principles of surfacing. Surfacing consumables*. Kiev, PWI, 7–11 [in Russian].
10. Som, A.I. (2016) Iron-based alloy for PTA surfacing of screw conveyors of extruders and injection molding machines. *The Paton Welding J.*, **7**, 21–25.
11. Gladky, P.V., Pereplyotchikov, E.F., Ryabtsev, I.A. (2007) *Plasma surfacing*. Kiev, Ekotekhnologiya [in Russian].

Received 25.03.2019

DOI: http://dx.doi.org/10.15407/tpwj2019.04.07

FORMATION OF METAL POOL IN CURRENT-SUPPLYING MOULD AT ELECTROSLAG PROCESS

Yu.M. KUSKOV and **T.I. GRISHCHENKO**
E.O. Paton Electric Welding Institute of the NAS of Ukraine
11 Kazimir Malevich Str., 03150, Kyiv, Ukraine. E-mail: office@paton.kiev.ua

Results of experiments were presented on study of the effect of different technological parameters on the formation of a metal pool in electroslag surfacing with a discrete filler either in the form of electrode or no-current large-section billet in current-supplying mould. It was found that the metal pool shape can be affected by changing the electric mode of the process, electrical scheme of connection of the current-supplying mould using direct and alternating current. The ways of producing a favorable metal pool shape at increased efficiency of the electroslag process are shown. 8 Ref., 2 Tables, 2 Figures.

Keywords: *circumferential and edge electroslag surfacing, current-supplying mould, metal pool*

Volume and shape of the metal pool are among those factors, determining the metal quality both of the ingots, as well as deposited layers, produced during electroslag melting of consumable electrodes in a conventional water-cooled mould [1–3]. In electroslag surfacing (ESS) the depth and uniformity of base metal penetration depend on the metal pool shape. At its more shallow shape, the probability of producing quality mixing of metals is increased in a number of cases.

The same factors are also important for the metal, solidifying in a current-supplying mould (CSM). In spite of design differences of CSM from a conventional mould (4–7) and, respectively, another conditions of distribution of electric current in a slag pool (independently of type of metal being remelted), the solidification of metal in a CSM forming section is governed by the same laws) [8].

The aim of the present work is to evaluate the effect of technique and technology of electroslag surfacing in CSM on formation of pool of metal being remelted. During investigations the following techniques and technologies were considered: surfacing with electrodes or no-current large-section billets or a discrete filler, making of edge or circumferential surfacing, application of different schemes of CSM connection, application of one or two DC or AC power sources.

During the edge surfacing, the CSM of 180 mm diameter and steel electrodes or no-current billets of steel X70 of 40–130 mm diameter, as well as chips of low-alloy steel after milling were used. The circumferential ESS of 100 and 150 mm diameter parts was performed by 2–3 mm diameter shots of non-alloyed and chromium cast iron in CSM of 200 and 250 mm diameter, respectively. Power sources were transformers TShP-10 and TShS-3000-1, as well as rectifiers VDM-5000 and VDU-1202. Electrical schemes of CSM connection in electroslag process using a discrete filler and electrodes (billets) are given in Table 1.

Electrical mode of surfacing was selected with account for a stable electroslag process.

The electroslag process was started at a «solid» start (by means of a water-cooled electrode with a graphite headpiece) or at a «liquid» start (flux was melted in a graphite crucible). The working fluxes were AN-75, ANF-29, ANF- 32.

The shape of a metal pool bottom was fixed by introducing the portions of solid alloy granules or chromium cast iron shots of a fine fraction into a molten metal, supplied to the slag pool surface during surfacing of steel layers.

In some cases the bottom shape was set by a special etching of deposited metal to determine the direction of crystal growth and location of liquid phase surface, corresponding to it.

The macrosections of specimens, produced at the edge and circumferential electroslag deposits with a discrete filler and large-section electrode, are shown in Figure 1.

As is seen from Figure 1, during the edge ESS the metal pool shape, produced due to metal of the molten filler, has a specific shape of a «sombrero» type with a peak in center of a layer deposited and depressions along its edges. This shape is defined by a CSM design and, respectively, by a special distribution of electric current in slag and metal pools (Figure 2). Reduction in difference of heights of peak and depression parts of the layer can be attained by applying special technological procedures.

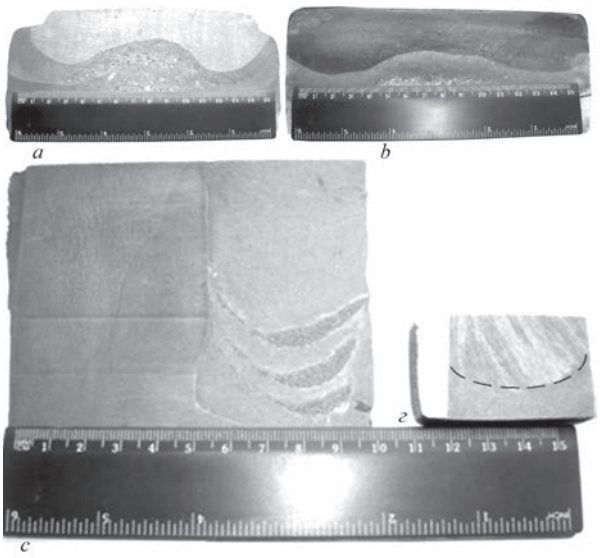

Figure 1. Longitudinal macrosections from specimens, deposited by different technologies: edge surfacing with low-alloy steel chips by electric scheme 1 (*a*) and with large-section electrode by electric scheme III, electrode $Ø_{el}$ = 90 mm (*b*); circumferential surfacing by nonalloyed (*c*) and chromium cast iron (*d*) shots by electric scheme Ia

In case of application of consumable electrodes (billets) during edge ESS the pool shape can also be corrected, which will be discussed below.

During the circumferential ESS with a discrete filler the metal pool shape is similar to the shape, produced in surfacing with a large-section electrode (for example, tubular electrode) and can be changed both due to the electric mode of surfacing and also by the mass rate of filler feeding into the slag pool.

The effect of a kind of current used, electric scheme of CSM connection and diameter of consumable elec-

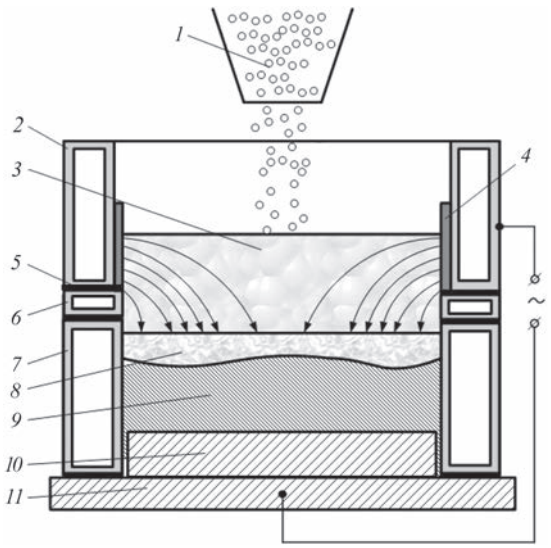

Figure 2. Scheme of distribution of electric current in slag and metal pools in edge ESS in CSM: *1* — discrete filler; *2*, *6*, *7* — current-carrying, intermediate and forming sections of mould, respectively; *3* — slag pool; *4* — protective lining; *5* — insulating gasket; *8* — metal pool; *9* — deposited metal; *10* — workpiece; *11* — bottom plate

Table 1. Electric schemes of CSM connections during electroslag process with use of a discrete filler and large-section electrodes (billets)

Designation of scheme	Electric scheme of CSM connection
I, Ia	TShP-10 / TShP-10
II	TShP-10
III	TShP-10
IV	TShS 3000-1, TShP-10
V	TShP-10, A, Б, TShS 3000-1
VI	TShP-10, B, A, TShS 3000-1
VII	VDM-5000
VIII	VDM-5000
IX	VDM-5000
X	VDU-1202, VDM-5000

Table 2. Shape of metal pool bottom under different conditions of edge ESS process with large-section electrode (billet)

Number of experiment	Kind of current	Type of metal remelted (electrode/billet)	Diameter of electrode/billet, mm	Designation of electric scheme	ESS parameters		Shape of metal pool bottom
					Current at CSM, kA	Efficiency, kg/h	
8M	Alternating	Electrode	90	II	1.5–2.5	9	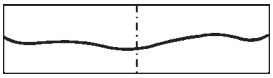
9M	Same	Same	130	II	1.5–3.5	17	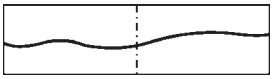
14M	»	»	40	III	1.4–2.2	39	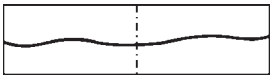
16M	»	»	90	III	1.6–3.1	39	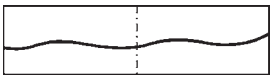
18M	»	»	90	Conventional ESR	2.1–2.8	51	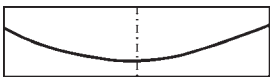
21M	»	»	130	III	3.0–3.3	136	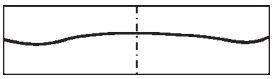
22M	»	»	90	III	2.4–3.0	50	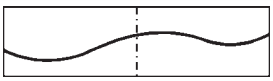
23M	»	»	40	III	1.9–2.6	34	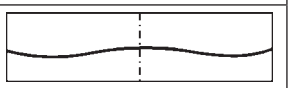
24M	»	»	90	IV	1.9–2.0	7	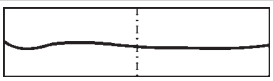
25M	»	»	90	V	1.9–3.7	42	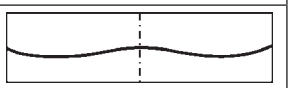
26M	»	»	90	VI	1.0–2.2	27	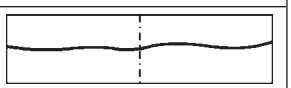
29M	»	»	40	VII	1.8–2.6	24	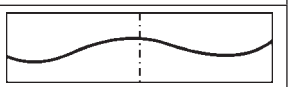
30M	»	»	130	VI	2.0–3.3	70	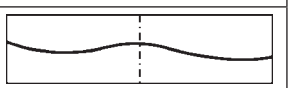
39M	Direct	Billet	90	VII	2.6–2.8	20	
44M	Same	Electrode	90	VIII	1.0–1.6	39	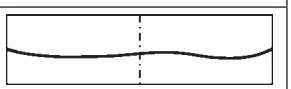
46M	»	Same	90	IX	1.6–2.5	21	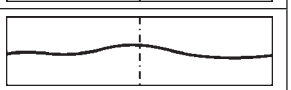
47M	»	»	90	X	1.0–1.1	69	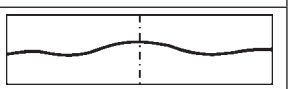

trode (billet) on metal pool shape at edge ESS is given in Table 2.

For comparison, the pool shape produced by remelting (ESR) of electrode in the same forming section of CSM of 180 mm diameter, at disconnection of its current-carrying section from the power source, i.e. transformation of CSM into conventional mould (experiment number is 18M) is presented.

From the results of experiments, presented in Table 2, the following conclusions can be made:

• it is possible to produce the most shallow shape of metal pool by use of one DC power source;

• use of two DC power sources complicates the surfacing technology, somewhat deteriorates the pool shape, but allows increasing the process efficiency by 1.5–2.0 times at a relatively low current, supplied to the mould current-carrying section;

• melting of nocurrent billet in slag pool, heated by passing of electric current in it, allows producing a shallow shape of metal pool, but this technology is characterized by a low efficiency of the electroslag process;

• at alternating current, which is the most frequently applied in electroslag processes, it is possible to provide the pool shape, comparable with a shape, attained in DC electroslag process;

• at the CSM connection scheme to one AC power source it is possible to produce the relatively shallow pool shape at different diameters of consumable electrodes;

• at the scheme with one AC power source for producing an optimum ratio of the pool shape characteristics and process efficiency it is preferable to apply the variant with different potential at electrode and workpiece.

1. (1986) *Metallurgy of electroslag process*. Ed. by B.E. Paton, B.I. Medovar. Kiev, Naukova Dumka [in Russian].
2. Iu, K.O., Doming, J.A., Flanders, H.D. (1987) Macrosegregation in Inconel 718 alloy, produced by ESR and VAR. Electroslag remelting: Issue 9. In: *Proc. of 8th Int. Conf. on Vacuum Metallurgy, Special Types of Melting and Metallurgical Coatings* (Linz, Austria, 30.09–4.10.1985), 164–170.
3. Chumakov, I.V., Pyatygin, D.A. (2006) Peculiarities of electroslag remelting at direct current with rotation of consumable electrode. *Izv. Vuzov. Chyorn. Metallurgiya*, **3**, 22–25 [in Russian].
4. Ksendzyk, G.V., Frumin, I.I., Shirin, V.S. (1981) *Electroslag remelting and surfacing apparatus*. USA, Pat. 4.305.451.
5. Kuskov, Yu.M. (2006) Resource-saving technology of restoration and manufacture of parts by electroslag surfacing method. *Tekhnologiya Mashinostroeniya*, **6**, 40–42 [in Russian].
6. Ksendzyk, G.V., Frumin, I.I., Shirin, V.S. (1980) *Electroslag remelting and surfacing apparatus*. USA, Pat. 4.185.682.
7. Kuskov, Yu.M., Soloviov, V.G., Lentyugov, I.P. Zhdanov, V.A. (2018) Role of slag pool in process of surfacing in current-carrying mould. *Sovrem. Elektrometall.*, **2**, 41–44 [in Russian].
8. Kubin, M., Scheriau, A., Knabl, M., Holzgruber, H., Korp, Y. (2016) Investigation of the implication of the current conductive mould technology with respect to the internal and surface quality of ESR ingots. In: *Proc. of Medovar Memorial Symposium* (Ukraine, Kyiv, 7–10 June, 2016), 174–179.

Received 06.03.2019

Calendar of April

APRIL 1, 1938 Tirpitz, the second Bismarck-class battleship was launched. It was part of Kriegsmarine (Germany). The ship practically did not take part in combat operation, but by its presence in Norway it threatened the Arctic convoys to the USSR and contained considerable forces of the British fleet. This battleship was characterized by a large scope of welding application in its construction. The ship hull was welded for approximately 90–95 %. This allowed a significant reduction of the ship weight, compared to application of rivets, and this, in its turn enabled creating more powerful armour protection.

APRIL 2, 1924 Birthday of A.S.Demianchuk (1924–1990), representative of the Paton school. Invented and build under his guidance, the high-frequency condensed spark generator with shock excitation enabled development of ingenious procedures for spectral analysis of various steels, welded joint metal, composite materials and diffuse coatings. The procedure was successfully introduced into practical work of spectral laboratories of research institutes and central plant laboratories. A.S. Demianchuk is the author of about 100 scientific works.

APRIL 3, 1984 In 1984 Rakesh Sharma, as a member of the international space crew, conducted the «Overcooling» experiment in the PWI developed coating unit «Isparitel-M». Rakesh Sharma is the first Indian cosmonaut and 138th man in the world, who made a space flight. Melting and solidification of spherical castings moving freely in weightlessness and vacuum was performed during the experiment. These experiments were very important for development of welding technologies in space.

APRIL 4, 1973 Construction of the World Trade Center in New York was over. During its erection, 139500 kg of metal deposited at welding, was used. The complex of seven buildings was designed by architect Minoru Yamasaki. The architectural dominant of the complex were two towers, each of which had 110 stories — the North (417 m high) and the South (415 m high). The buildings were designed as a «tube-frame» structural system. The «tube-frame» principle was a new approach, which allowed increasing the usable area space, unlike the traditional design (the towers were destroyed on September 11, 2001 during a terrorist attack).

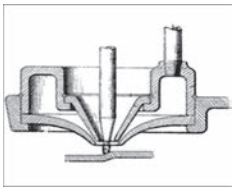

APRIL 5, 1927 (publication date) A plasma torch or plasmatron in principle is an electrode, connected to a current source and surrounded by a nozzle with a channel of a comparatively small diameter. The second potential of the source is connected to the torch nozzle or to the item. In 1921 Himes, US inventor, applied a torch of such a design for cutting metals, achieving a high concentration of heat, powerful gas pressure and good quality of the cut. The history of plasma welding begins exactly from this moment. Himes torch was a prototype of modern plasmatrons. The term «plasma» proper was introduced by scientist Irving Langmuir (1881–1957).

APRIL 6, 1890 Birthday of Anton Herman Herard (Antony) Fokker (1890–1939), Dutch aircraft designer. In 1913 he founded an aircraft factory near Schwerin (Germany). During the First World War Anthony Fokker began applying welding in the production of fuselages of German fighters. The improved Fokker E.I. aircraft made its first flight in the spring of 1914, and in a year it was already batch produced and widely used at the fronts. In 1920s Anthony Fokker moved to the USA, where he founded a subsidiary of his company. Fokker Company became one of the leading manufacturers of civil aircraft in the world. In 1926 the flight over the North Pole was made in one of Fokker aircraft.

APRIL 7, 1947 Henry Ford (1863–1947) died. He was an US industrialist, owner of car factories all over the world, author of 161 US patents. Henry Ford organized mass production of cars on an assembly line, and focused on application of resistance, arc and gas welding instead of forge welding and riveting. The design of the chassis, bodies, exhaust pipes, tanks and a number of other assemblies and parts was created already taking into account the welding technology capabilities. Chassi in the form of a frame was welded by oxyacetylene flame at first, and then by consumable electrode arc. A significant part of the joints were made by resistance butt, seam and spot welding.

*The material was prepared by the Steel Work Company (Krivoy Rog, Ukraine) with the participation of the editorial board of the Journal. The Calendar is published every month, starting from the issue of «The Paton Welding Journal» No.1, 2019.

APRIL 8, 1919 Birthday of Yu.N. Gotalsky (1919–2002) — famous scientist, representative of the Paton school. Results of scientific works of Yu.N. Gotalsky allowed development of consumables for welding dissimilar steels, which are widely used even now. They are applied for realization of a fundamentally new welding technology, namely without preheating or heat treatment of pipes for petrochemical and power engineering industry. In PRC, electroslag welding was applied with the participation of Yu.N. Gotalsky for welding forging dies, steam boilers, rolling and other equipment already by the end of 1959. Yu.N. Gotalsky is author of 2 monographs, more than 130 papers and author's certificates.

APRIL 9, 1939 Birthday of B.V. Danilchenko — representative of the Paton school, one of the developers of the technology of wear-resistant arc surfacing of plates by flux-cored strips. He personally and as a co-author developed and put into industrial production a series of consumables for surfacing special steels and alloys, and deposition of protective thermal coatings, and created a number of technologies for surfacing various industrial parts. V.D. Danilchenko is author and co-author of about 130 scientific works and more than 40 author's certificates.

APRIL 10, 1870 Birthday of Max Ulrich Schoop (1870–1956) — developer of the method of thermal spraying of metal (metallizing). This process is related to welding. Welding joins metal elements, and thermal spraying protects surfaces from corrosion, wear, etc. Schoop's first machine transferred liquid lead using water steam. In 1913 Ulrich Schoop improved and patented the design of gas-flame sprayer, where spraying material was fed into gas torch flame in the form of wire. Owing to his significant contribution to initial development of the technologies, the methods of thermal coating deposition by spraying began to be called schooping, by the name of inventor of the technology.

APRIL 11, 1999 Birthday of S.I.Semergeev (1925–1999) — representative of Paton school. He studied the process of capacitor-type seam welding, developed the technology and equipment for application of this process in the enterprises of different industrial sectors. S.I.Semergeev studied the dependencies of mode parameters on the thickness and thermophysical properties of materials, in particular, chemically active and refractory alloys in similar and dissimilar joints. He developed technologies of welding coiled materials in metallurgical production, sealing of sensitive elements and vacuum tubes in instrument-making and radioelectronics.

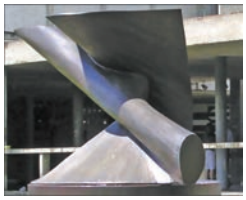

APRIL 12, 1962 Antoine (Nota Berkovich) Pevzner (1884–1962) died. He was a Russian and French artist and sculptor. In 1911 he moved to Paris, where he met A.P. Arkhipenko (1867–1964) and A. Modiliani (1864–1920). Developing the ideas of constructivism, he came to kinetic art. Pevzner's studio was at the outskirts of Paris, which is where his sculptures are located. He was one of the first artists, who used the soldering lamp to create sculptures, welding copper rods onto a sculptural form, and developed several methods which can be used in welding when creating sculptural forms.

APRIL 13, 1961 Birthday of A.M.Beinish (1911–1997) — representative of Paton school. He took an active part in development of highly-productive electrodes of ANO-1 grade with ferrous powder in their coating, low-hydrogen electrodes ANP-6P and ANO-31, technologies of commercial production of electrodes and their application at Nizhniy Tagil and Kremenchug carriage works.

APRIL 14, 1928 Academician E.O. Paton founded the Welding Laboratory at the All-Ukrainian Academy of Sciences in Kiev. Having considerable experience, he put together a comprehensive program of investigations aimed at development of materials and equipment, promising methods and technologies of welding critical engineering facilities. The very first studies performed by the Laboratory aroused interest both in the USSR, and abroad. In 1930 E.O. Paton organized the Electric Welding Committee — a public organization, the main objective of which was coordination of the activities of enterprises and institutions, involved in welding production.

APRIL 15, 1939 Birthday of L.A. Semenov (1939–2013) — representative of the Paton school. He directly participated in performance of a package of research and technology work in the field of flash-butt welding of aluminium alloys. Technologies and equipment for welding the load-carrying elements (frames and shells) of flying vehicle bodies were developed and successfully introduced at the enterprises of the Ministry of Aviation Industry, Defense Industry and General Machine-Building of the former USSR. L.A. Semenov was involved in development of the technology of welding new components and parts of Zenith and Cyclone-4 carrier rocket bodies.

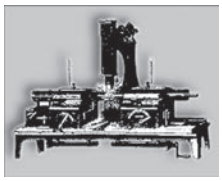

APRIL 16, 1889 (information) A fundamentally new relative position of electrodes, item being welded and arc was proposed. Ch.A. Coffin, Manager of American Electric Company, patented a roller metal electrode, moving above the item surface on a carriage insulated from it. The arc was excited between the rotating roller electrode (positive potential), and item connected to negative potential. Ch.A. Coffin used the same carriage for fastening two carbon electrodes located on both sides from the weld axis.

APRIL 17, 1938 Birthday of A.A. Zagrebelny (1939–2012) — representative of Paton school, specialist in the field of space technologies and structures. He took an active part in development of «Isparitel», «Isparitel-M», «Yantar» units, which operated in 1976–1989 on board the «Salyut» and «Mir» space stations. He is one of the developers of a versatile electron beam hand tool, which was used in 1984 at «Salyut-7» station to perform the world's first experiments on welding, cutting, brazing and coating in open space.

APRIL 18, 1932 Birthday of V.F. Lapchinsky (1932–1997) — representative of Paton school, organizer and participant of the work in the field of welding and related technologies for space environment. He participated in preparation of important experimental studies in space and development of unique hardware, including «URI», «Universal», «Isparitel», «Yantar» units, used to perform experiments on welding and related technologies in open space.

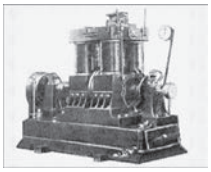

APRIL 19, 1892 One of Henry Howard's patents was registered. Based on a number of patents, the designer created the first stationary welding machine and introduced it at the factories of Lloyd&Lloyd Company in Birmingham in 1887. It consisted of four dynamo machines (500 A, 150 V), actuated by a steam engine, 1800 «Benardos accumulators» and ballast rheostats. A little later N.G. Slavyanov came up with a novel idea in those times — to eliminate the storage battery from the welding circuit. It was implemented at Perm cannon works at manufacture of two powerful DC dynamo machines (300 and 100 A).

APRIL 20, 1938 Birthday of V.Ya. Saenko (1938–2015) — representative of Paton school, renowned expert in the field of electrometallurgy, in particular, electroslag technologies for remelting, casting, welding of steels and alloys, and production of unique items for many industries. V.Ya. Saenko is the author and coauthor of about 320 scientific works, and about 300 author's certificates and patents.

APRIL 21, 1958 During the Brussels World Exhibition in 1958 the Soviet Union announced development of electroslag welding. The method of electroslag welding (ESW) was developed by PWI staff members at the beginning of 1950s. ESW is one of the variants of fusion welding. It is based on heat evolution at electric current flowing through liquid slag that enables melting the edges of parts to be welded and the filler metal, as well as maintaining a high temperature of the melt. This welding process opened up great possibilities in production of heavy metallurgical, forging and other equipment.

APRIL 22, 1886 Construction of the Statue of Liberty, one of the most famous sculptures in the world, was over. It was a present of French citizens for the one hundredth anniversary of the American Revolution. The metal frame of the Statue was attached to the central pylon, welded from four metal columns by autogenous welding. Spiral metal staircases were mounted around these columns, which consisted of 168 steps each. The Statue metal frame is covered by three hundred copper plates, fastening which required about 300 thousand copper rivets. Total weight of copper used for Statue facing is 31 t, and total weight of its steel structure is 125 t. The construction was installed by Gaget & Gauthier Company.

APRIL 23, 1854 Birthday of N.G. Slavyanov (1854–1897) — Russian engineer, inventor of metal electrode electric arc welding. The inventor paid serious attention to mechanization and automation of electric arc welding. He made and tested the world's first semi-automatic welding machine — the «electric melter». An important technological feature of his welding method was mandatory automatic regulation of the electric arc length at application of metal electrode. His opinion of the impossibility of conducting metal electrode electric welding process without automatic regulation of the arc length was not confirmed later on: consumable electrode manual arc welding became quite extensively used.

APRIL 24, 2014 A sculptor under the pseudonym of TEJN installed one of his latest sculptures — «Reaching for Freedom». TJEN is the pseudonym of a contemporary Danish artist, who began his artistic work as a street artist in 2007. Making his works from metal and using welding, he became famous owing to unsanctioned creation of sculptures. Without permission of the authorities, the artist welds or chains the monument, wherever he wants. Later on the sculptures began to be returned to their places as architectural monuments. In his work the sculptor uses welding, cutting, surfacing and other methods of metal treatment. Today his works are often displayed at prestigious exhibitions.

APRIL 25, 1990 Discovery Shuttle STS-31 put the Hubble orbital telescope into orbit. Today it is one of the most up-to-date pieces of equipment for space research. Several welding technologies were used to create this complex apparatus. Laser welding was applied in manufacture of special light-weight cellular mirrors. In this connection, Welded Sheet Metal Speciality Co. should be mentioned, which was constantly involved in welding operations during fulfillment of major projects, such as creation of Hubble telescope, manufacture of Apollo spacecraft, construction of Nautilus submarine, and many others.

APRIL 26, 2012 Having covered 540 miles with tow boats, the sea ice-resistant off-shore platform (SOSP) «Prirazlomnaya» arrived at the home site in the Pechora Sea, where it was later on mounted into a common block afloat with application of underwater welding. Already on December 20, 2013 Gazprom Neft Shelf Company announced the start of oil production at SOSP «Prirazlomnaya». At present this is the only platform, driving oil on the Russian Arctic shelf. Platform construction required wide application of underwater welding. Welding was performed with 1.6 mm flux-cored wire PPS-EK1 (PWI development) in the vertical and overhead position with two semi-automatic machines PSP-3. Total length of welds was 1020 m.

APRIL 27, 1967 1967 World Exhibition opened, the Montreal Biosphere becoming its symbol. Built as a pavilion of US exposition at Expo-67 International Exhibition, the Biosphere became one of the symbols of the city of Montreal. The construction has the form of a large sphere, which consists of a multitude of parts joined by welding. Each of them looks like a special molecular compound, belonging to a particular class of the so-called allotropic forms of carbon, known to all. In May, 1976 during repair welding operations, the Biosphere dome caught fire, but, luckily, there were no casualties.

APRIL 28, 1972 By the end of April, 1972, welder G.G. Dochkin (1842–2013) mastered the technique of producing a range of colour shades on titanium alloys in TIG welding. Using this effect, G.G. Dochkin created a number of unique works of art, having no analogs. Today many of them are in private collections all over the world.

APRIL 29, 1897 Birthday of G.S.Shpagin (1897–1952) — Soviet designer of small arms. The designer became the most famous for development of a submachine gun of 1941 model (PPSh), the most mass automatic weapon of the Red Army during the Second World War. Stamped welded structures were widely used in its design, greatly simplifying its manufacture.

APRIL 30, 1941 Three types of vessels, including Liberty dry cargo ship, were selected at the end of April for building the US transport fleet. The first ship of this series — Patrick Henry was launched on September, 27, 1941 at Bethlehem-Fairfield shipyard (Baltimore County). In January 1943 there were already about 500 of them. Just during 1942, 500 thousand tons of steel were saved due to replacement of riveted structure and riveting technology by welded structure and welding of the ships. Construction cycle was reduced to 50 days.